Probabilistic Analysis of Flow in Random Porous Media by Stochastic Boundary Elements [1]

R. Valéry Roy, *Mechanical Engineering Department, University of Delaware, Newark, DE 19716*
and
Stéphan T. Grilli, *Ocean Engineering Department, University of Rhode Island, Narragansett, RI 02882, USA*

ABSTRACT

The mathematical and numerical modeling of groundwater flows in random porous media is studied assuming that the formation's hydraulic log-transmissivity is a statistically homogeneous, Gaussian, random field with given mean and covariance function. In the model, log-transmissivity may be conditioned to take exact field values measured at a few locations. Our method first assumes that the log-transmissivity may be expanded in a Fourier-type series with random coefficients, known as the Karhunen-Loève (KL) expansion. This expansion has optimal properties and is valid for both homogeneous and non-homogeneous fields. By combining the KL expansion with a small parameter perturbation expansion, we transform the original stochastic boundary value problem into a hierarchy of deterministic problems. To the first order of perturbation, the hydraulic head is expanded on the same set of random variables as in the KL representation of log-transmissivity. To solve for the corresponding coefficients of this expansion, we adopt a boundary integral formulation whose numerical solution is carried out by using boundary elements and the dual reciprocity (DR-BEM). To illustrate and validate our scheme, we solve three test problems and compare the numerical solutions against Monte Carlo simulations based on a finite difference formulation of the original flow problem. In all three cases we obtain good quantitative agreement and the present approach is shown to provide both a more efficient and accurate way of solving the problem.

1 INTRODUCTION

Due to the inherent non-uniformity of porous media in geologic formations and to the lack of complete knowledge of the medium at all locations of a large natural formation, it has long been recognized that flows in porous media could be more realistically treated as solutions of Boundary Value Problems (BVP) with random parameters (Freeze [2], Bakr *et al.* [4], Smith and Freeze [3], Dagan [6, 7, 10]). Uncertainties in the medium properties (e.g. hydraulic conductivity) and/or in initial

[1] *Engineering Analysis with Boundary Elements.*, submitted 04/96

and boundary conditions, however, result in uncertainties in the system output which must thus be predicted in a probabilistic framework. For instance, large-scale heterogeneity of natural formation is believed to be the cause of important discrepancies found between field measurements of solute transport and their numerical predictions based on deterministic models [9].

We consider here the numerical solution of steady-state saturated flows with specified boundary heads or normal fluxes in two-dimensional domains. Hence, we consider the problem at the so-called *regional scale*, that is, at the horizontal scale of an entire aquifer, so that the flow variables can be averaged over depth. The relevant property of the medium at this scale is the hydraulic transmissivity, that is, the hydraulic conductivity averaged over the entire depth of the domain. The equations relating hydraulic head, specific discharge, hydraulic transmissivity and recharge intensity are reviewed in Section 2.1. The medium is assumed bounded, non-uniform, isotropic, and statistically homogeneous, with hydraulic transmissivity T described as a homogeneous random field with (unconditional) log-normal probability density and specified spatial correlation (or covariance) function. We introduce the log-transmissivity $Y = \ln T$ and treat its modeling by unconditional or conditional probability densities. In the latter case, the modeling is based upon probabilities conditioned on a finite set of known (deterministic) values of Y at specific measurement locations. In this case, the transmissivity is necessarily a non-homogeneous random field.

In this paper, unlike in most earlier work, we do not solve the corresponding stochastic BVP's by a Monte Carlo technique, i.e., deterministically solving for a large number of output realizations associated with input realizations. Rather, we address the problem in a fully stochastic sense. To do so, our computational scheme first assumes that the medium log-transmissivity can be represented by a truncated Karhunen-Loève (KL) expansion on a discrete set of uncorrelated $N(0,1)$ Gaussian variables. The theoretical basis of KL expansion of random fields can be found in Papoulis [18]. Its use has been pioneered by Ghanem and Spanos[19] for the solution of stochastic BVP's. The KL expansion of random fields has very attractive properties and essentially amounts to a discretization of the field in the space of random events. Since it requires only the mean and covariance of the random field, it can be applied equally to homogeneous, as well as, non-homogeneous random fields and, hence, lends itself to conditional modeling (kriging) as shown in Section 2.2.

In Ghanem and Spanos[19], upon discretization of the spatial operators (for instance by finite elements), the original stochastic BVP is reduced to an algebraic system of equations in terms of a finite set of uncorrelated Gaussian variables. This system is subsequently solved by expanding the vector of nodal unknowns along a basis of Wiener-Hermite multivariate polynomials of the random variables at hand. We note that this approach cannot be adopted here due to the large number of terms that must be retained in the KL expansion for a medium characterized by small correlation scale. Instead, we have to resort to a perturbation scheme, that is, assume that the standard deviation σ_Y of the log-transmissivity is a small parameter. We then express the unknown potential as a perturbation expansion of this parameter. To the first order of perturbation, it is found in Section 2.3 that the potential can be discretized along the same set of random variables as the log-transmissivity. Hence, by combining the KL expansion with a perturbation expansion, we obtain a hierarchy of deterministic equations governing the coefficients of the perturbation expansion. Other types of perturbation solutions have of course been used in the past, for example in [4, 5, 7, 11], for the solution of flows in random porous medium.

In Section 3, we present a numerical scheme whereby the corresponding deterministic BVP's are spatially discretized and solved by a two-dimensional Boundary Element Method (BEM; Brebbia[14]), taking into account deterministic boundary conditions. Random boundary conditions may be accounted for in a similar way, but we are mainly interested in the more difficult problem of predicting the effects of the medium heterogeneity upon the flow. Domain integrations (some of them containing problem unknowns) appearing in the resulting integral equations are transformed into boundary integrals by using the Dual Reciprocity BEM approach (DR-BEM; e.g., Partridge *et al.*[16]). After numerically calculating boundary integrals, the resulting problems become algebraic systems of linear equations.

Finally, Section 4 is devoted to applications that illustrate our procedure. Three case problems with a simple square geometry and deterministic boundary conditions are treated in detail. In these problems, we employ a particular unconditional covariance function which leads to closed-form expressions of the KL expansion of the log-transmissivity. Our third example deals with a modeling of Y conditioned upon five measurement values. It should be stressed that our test cases do not assume a small value of the standard deviation σ_Y, so that the validity and accuracy of our proposed scheme must be tested by comparing the ensuing numerical results with those obtained by Monte Carlo simulations, based on a finite difference formulation of the original BVP.

2 THE MATHEMATICAL MODEL

2.1 Governing equations and boundary conditions for porous media flow

The steady flow of water, assumed homogeneous and incompressible, through a porous, isotropic and non-deformable medium is described by the macroscopic flow variables, $\mathbf{q}$, the specific discharge (or $\mathbf{u} = \mathbf{q}/n$, the velocity vector, n being the medium's porosity) and h the potential (hydraulic head), with $p = \rho g(h - z)$, the pressure. These quantities satisfy continuity equation (in the absence of recharge),

$$\nabla \cdot \mathbf{q} = 0 \tag{1}$$

and Darcy's law,

$$\mathbf{q} = -K \ \nabla h \tag{2}$$

where K is the hydraulic conductivity of the medium [1]. Here, K is a scalar function, that is, we assume that there exists no systematic anisotropy of the measured core samples. By eliminating $\mathbf{q}$ between Eqs. (1) and (2), we obtain an equation governing the potential h,

$$\nabla \cdot (K \ \nabla h) = 0. \tag{3}$$

This equation, with proper boundary conditions, is relevant at the so-called *local scale*, that is, at the scale of the formation thickness in both horizontal and vertical directions. Hence, at this scale, the problem must be treated as three-dimensional. However, in a stochastic context, it is possible to obtain effective properties of the medium, i.e., to relate the mean macroscopic variables $\bar{h}$ and

$\bar{\mathbf{q}}$ through an average Darcy equation,

$$\bar{\mathbf{q}} = -K_{ef}\ \boldsymbol{\nabla}\bar{h} \tag{4}$$

where K_{ef} is referred to as the effective conductivity of the medium.

At the *regional* scale, that is, at the horizontal scale L of an entire aquifer considered much larger than the formation thickness D, it is possible to reduce the problem to a two-dimensional one by integrating continuity equation and Darcy's law over depth. Hence, potential and hydraulic conductivity become functions of only the planar coordinates $\mathbf{x} = (x_1, x_2)$. It can be shown that, if K is replaced by the transmissivity $T = DK_{ef}$, and the potential h by $\phi = \bar{h}$, the governing Eq. (3) now reads,

$$\boldsymbol{\nabla}\cdot(T\ \boldsymbol{\nabla}\phi) = -R \tag{5}$$

where we have included a recharge R to account for infiltration or leakage, and pumping or recharging wells. By introducing the log-conductivity $Y = \ln T$, this equation can be rewritten as

$$\nabla^2\phi\ + \boldsymbol{\nabla}Y\cdot\boldsymbol{\nabla}\phi = -R\, e^{-Y} \tag{6}$$

Hence, the *direct* problem consists of solving Eq. (6) over a domain Ω, given the medium log-transmissivity Y and relevant boundary conditions on boundary Γ, such as the Dirichlet condition,

$$\phi = \phi_b \qquad\qquad \text{on } \Gamma_d \tag{7}$$

for the specification of a hydraulic head ϕ_b, and the Neumann condition,

$$\frac{\partial\phi}{\partial n} = \frac{\partial\phi_b}{\partial n} \qquad\qquad \text{on } \Gamma_n \tag{8}$$

for the specification of a normal flow velocity—including the case of impermeable boundaries with zero normal velocity—, with $\Gamma = \Gamma_d \cup \Gamma_n$ (Fig. 1).

Numerous field data show that T is not a smooth, slowly-varying function of space, and that, as a rule, aquifers are heterogeneous. The next section provides a mathematical characterization of Y.

2.2 Representation of stochastic fields

We assume that the log-transmissivity Y varies in space and is subjected to uncertainty. Hence we treat $Y(\mathbf{x})$ as a *random field*, that is, at each location $\mathbf{x}_i \in \Omega$ the quantity $Y(\mathbf{x}_i, \omega)$ is regarded as a random variable, where the realization ω is considered an element of the space of random events (this notation will be omitted whenever needed). To completely describe the probabilistic structure of $Y(\mathbf{x}, \omega)$, we need to specify the infinite sequence of unconditional joint probability density functions (p.d.f.),

$$p^{(n)}_{Y(\mathbf{x}_1),Y(\mathbf{x}_2),\ldots,Y(\mathbf{x}_n)}(y_1, y_2, \ldots, y_n)$$

for $n = 1, 2, \ldots$, and for all locations $\mathbf{x}_i$ of Ω. By assuming that the field is *Gaussian* and *statistically homogeneous*, its p.d.f. can be entirely defined by the mean $m_Y = \mathrm{E}[Y(\mathbf{x}, \omega)]$ (constant over Ω) and covariance $K_Y(\mathbf{x},\mathbf{x}') = \mathrm{E}[Y'(\mathbf{x},\omega)Y'(\mathbf{x}',\omega)] = \sigma_Y^2 \rho_Y(\mathbf{x}-\mathbf{x}')$, with $Y' = Y - m_Y$ (the random fluctuation part of Y). Here, σ_Y and ρ_Y denote the standard deviation of the field, constant over Ω, and the correlation coefficient, a function of the separation vector $\mathbf{r} = \mathbf{x}-\mathbf{x}'$ between two locations $\mathbf{x}$ and $\mathbf{x}'$, respectively. The operator $\mathrm{E}[\cdot]$ is the expected value, that is the ensemble average over all possible realizations of the random variable it acts upon. The restriction of homogeneity of Y may be somewhat relaxed by assuming that only the fluctuation $Y' = Y - m_Y$ is homogeneous and, hence, allowing a trend (or drift) in terms of a non-constant mean field $m_Y(\mathbf{x})$.

The log-normal property of the transmissivity is well-supported by field measurements at both the local and regional scales, and various models of covariance functions for Y have been proposed in the literature (Dagan [10]). The key parameters in these models are the correlations scales in the two spatial horizontal directions, which are proportional to the integral scales,

$$I_1 = \frac{1}{\sigma_Y^2}\int_0^\infty K_Y(r_1,0)dr_1, \quad I_2 = \frac{1}{\sigma_Y^2}\int_0^\infty K_Y(0,r_2)dr_2. \tag{9}$$

If L_1 and L_2 are characteristic length scales of the domain Ω in the x_1 and x_2 directions, then the ratios I_1/L_1 and I_2/L_2 are measures of the level of heterogeneity of the medium. We denote $I_Y/L = \min(I_1/L_1,\ I_2/L_2)$.

A key ingredient in our work, is the representation of the random field as a Karhunen-Loève (KL) expansion, a type of Fourier expansion for random functions, which amounts to a discretization in the space of random events[18],

$$Y(\mathbf{x},\omega) = m_Y(\mathbf{x}) + \sigma_Y \sum_{n=1}^{\infty} \xi_n(\omega)\,\lambda_n^{1/2}\, f_n(\mathbf{x}) \tag{10}$$

in which the set $\{\xi_n(\omega)\}$ denotes $N(0,1)$ uncorrelated Gaussian random variables, i.e., with zero mean, $\mathrm{E}[\xi_n] = 0$, and covariance $\mathrm{E}[\xi_m\xi_n] = \delta_{m,n}$, and where the functions $\{f_n(\mathbf{x})\}$ and scalars $\{\lambda_n\}$ denote sets of deterministic eigenfunctions, orthonormal over domain Ω, and eigenvalues, respectively, of the kernel ρ_Y, that is, the solutions of the integral equation,

$$\int_\Omega \rho_Y(\mathbf{x}-\mathbf{x}')f(\mathbf{x}')d\mathbf{x}' = \lambda f(\mathbf{x}) \tag{11}$$

where $\rho_Y(\mathbf{x}-\mathbf{x}')$ is the specified spatial correlation coefficient of the field Y. Note that the expansion on the first k functions of any other set of orthonormal functions will lead to an error greater than the one incurred by the first k KL functions $\{f_n(\mathbf{x})\}$.

In the applications, we will use the following exponential spatial covariance function for Y which is representative of some field measurements (Dagan [10]),

$$K_Y(\mathbf{x},\mathbf{x}') \equiv K_Y(\mathbf{r}) = \sigma_Y^2\rho_Y(\mathbf{r}) = \sigma_Y^2\ \exp\left(-\frac{|r_1|}{b_1} - \frac{|r_2|}{b_2}\right) \tag{12}$$

in which $\mathbf{r} = \mathbf{x}-\mathbf{x}' = (r_1,r_2)$. Note that this model is anisotropic even if the correlation scales b_1 and b_2 are chosen equal. For a rectangular domain, the corresponding eigenfunctions and eigenvalues can be found in closed form and are given in Section 4.2; other covariance models over more realistic domains, however, can be chosen, the corresponding eigenproblems (11) will then have to be solved by straightforward numerical techniques.

The KL representation of Y can be extended to the case of conditional modeling which accounts for the actual measured values of Y at a finite set of locations in Ω. Hence, the uncertainty at these points is kept at zero, while the overall uncertainty at all the other points is reduced as compared to that produced by the unconditional modeling. This form of stochastic interpolation (also referred to as *kriging* [12]) is well known in geostatistics and its benefits have been demonstrated by Dagan [7, 10]. Assuming that Y has been measured at M points $\mathbf{x}_j$, $j = 1, 2, ..., M$ of Ω, the data $Y(\mathbf{x}_j) = Y_j$ constitutes a realization of Y. By using statistical inference techniques, it is then possible to estimate the corresponding unconditional probabilities and the unconditional statistics for Y, i.e., m_Y, σ_Y, and $K_Y(\mathbf{r})$, the statistical quantities first introduced in this section. The realizations of the unconditional modeling of Y at the measurement points are compatible but yield different values than the measured values $Y(\mathbf{x}_j) = Y_j$. However, it is possible to estimate the statistical properties of Y conditioned on the measured data, so that the realizations of Y take the exact values $Y(\mathbf{x}_j) = Y_j$ and display uncertainty at all points other than the points of measurement. Assuming that the unconditional p.d.f.'s of Y are Gaussian, it can be shown that [7] :

- the conditional mean of Y is given by,

$$m_Y^{(c)}(\mathbf{x}) = \mathrm{E}[Y(\mathbf{x}|\mathbf{x}_1, \mathbf{x}_2, \ldots, \mathbf{x}_M)] = m_Y(\mathbf{x}) + \sum_{j=1}^{M} \mu_j(\mathbf{x}) \left(Y(\mathbf{x}_j) - m_Y(\mathbf{x}_j)\right) \tag{13}$$

where m_Y is the unconditional mean of Y;

- assuming homogeneity in the unconditional covariance, the coefficients μ_j are solutions of the linear systems,

$$\sum_{j=1}^{M} \mu_j(\mathbf{x}) K_Y(\mathbf{x}_j - \mathbf{x}_i) = K_Y(\mathbf{x} - \mathbf{x}_i) \qquad (i = 1, \ldots, M) \tag{14}$$

where K_Y is the unconditional covariance;

- the conditional covariance at two arbitrary points $\mathbf{x}$ and $\mathbf{x}'$ is given by,

$$\begin{aligned} K_Y^{(c)}(\mathbf{x}, \mathbf{x}') &= K_Y(\mathbf{x}, \mathbf{x}'|\mathbf{x}_1, \mathbf{x}_2, \ldots, \mathbf{x}_M) = K_Y(\mathbf{x} - \mathbf{x}') - \sum_{i=1}^{M} \mu_i(\mathbf{x}) K_Y(\mathbf{x}' - \mathbf{x}_i) \\ &= K_Y(\mathbf{x} - \mathbf{x}') - \sum_{i=1}^{M} \sum_{j=1}^{M} \mu_i(\mathbf{x}) \mu_j(\mathbf{x}') K_Y(\mathbf{x}_i - \mathbf{x}_j). \end{aligned} \tag{15}$$

We note that the conditional random field Y is not homogeneous, i.e., the conditional covariance depends on the positions $\mathbf{x}$ and $\mathbf{x}'$ and not on the difference $(\mathbf{x} - \mathbf{x}')$. The conditional mean is not a constant function, even if the unconditional mean is assumed constant. Conditioning causes a variance reduction, that is, $\sigma_Y^{(c)}(\mathbf{x}) \leq \sigma_Y(\mathbf{x})$. The equality is approached for points far from the measurement points, i.e. for $|\mathbf{x} - \mathbf{x}_i| \gg I_Y$. At the measurement points $m_Y^{(c)}(\mathbf{x}_i) = Y(\mathbf{x}_i)$ and $\sigma_Y^{(c)}(\mathbf{x}_i) = 0$ for $i = 1, \ldots, M$, i.e., the interpolator is exact. For a dense distribution of measurement points, i.e., at distances much smaller than the integral scale, the conditional variance approaches zero and the interpolator tends to be deterministic.

Given expressions of the unconditional KL eigenfunctions $\{f_n(\mathbf{x})\}_{n\geq 1}$ and eigenvalues $\{\lambda_n\}_{n\geq 1}$, the problem is to find the conditional KL sets. First, the functions $\{\mu_i(\mathbf{x})\}_{1\leq i\leq M}$ can be expressed as,

$$\mu_i(\mathbf{x}) = \sum_{k=1}^{\infty} \mu_{i,k} f_k(\mathbf{x}) \tag{16}$$

Given the following expansion of the covariance function,

$$K_Y(\mathbf{x},\mathbf{x}') = \sum_{k=1}^{\infty} \lambda_k f_k(\mathbf{x}) f_k(\mathbf{x}') \tag{17}$$

we find that the coefficients $\{\mu_{i,k}\}_{1\leq i\leq M}$ are solution of the linear systems (substitute Eqs. (16) and (17) in Eq. (14)),

$$\mathbf{K}\left\{\begin{array}{c} \mu_{1,k} \\ \vdots \\ \mu_{M,k} \end{array}\right\} = \lambda_k \left\{\begin{array}{c} f_k(\mathbf{x}_1) \\ \vdots \\ f_k(\mathbf{x}_M) \end{array}\right\} \quad k = 1, 2, \ldots \tag{18}$$

where $\mathbf{K}$ is the $M \times M$ symmetric covariance matrix of elements $k_{ij} = K_Y(\mathbf{x}_i, \mathbf{x}_j)$.

Similarly, expanding the conditional eigenfunction $f^{(c)}(\mathbf{x})$, solution of the integral equation,

$$\int_\Omega K_Y^{(c)}(\mathbf{x},\mathbf{x}') f^{(c)}(\mathbf{x}') d\mathbf{x}' = \lambda^{(c)} f^{(c)}(\mathbf{x}) \tag{19}$$

on the set of unconditional eigenfunctions, we obtain,

$$f^{(c)}(\mathbf{x}) = \sum_{k=1}^{\infty} \alpha_k^{(c)} f_k(\mathbf{x}) \tag{20}$$

Then, by substitution in Eq. (15), we find that $(\{\alpha_k^{(c)}\}, \lambda^{(c)})$ is solution of the algebraic eigenvalue problem,

$$\left(\mathbf{A} - \lambda^{(c)}\mathbf{I}\right)\left\{\begin{array}{c} \alpha_1^{(c)} \\ \alpha_2^{(c)} \\ \vdots \\ \alpha_L^{(c)} \end{array}\right\} = \mathbf{0} \tag{21}$$

where the elements of the $L \times L$ matrix $\mathbf{A}$ are given by ,

$$a_{kl} = \lambda_k \delta_{kl} - \sum_{i,j=1}^{M} k_{ij} \mu_{ik} \mu_{jl} \tag{22}$$

and where the level of truncation in expansion (16) must also be chosen as L. This approach will be illustrated in Section 4.2. More general techniques may be employed to solve the conditional eigenproblem (19), especially if closed-form expressions of the unconditional eigenfunctions are not available. It is evident that the representation (20) of the conditional KL functions $f_k^{(c)}$ in terms of the unconditional functions f_k may not lead to the most efficient numerical solution. The important point here is that KL expansions are not restricted to homogeneous random fields, but also apply to non-homogeneous fields as produced by conditional modeling.

2.3 Perturbation expansion: solution of a hierarchy of stochastic problems

Assume that the log-transmissivity admits a KL expansion in the form of Eq. (10). Here, the mean field m_Y, the KL eigenfunctions $\{f_k\}$ and eigenvalues $\{\lambda_k\}$ refer to unconditional, as well as conditional modeling of Y. In the unconditional case, the standard deviation $\sigma_Y = \sigma_Y^{(u)}$ is a constant. In the conditional modeling, the standard deviation $\sigma_Y^{(c)}$ is proportional to $\sigma_Y^{(u)}$, and ranges from of a value of zero (at the measurement locations) to the maximum value approaching $\sigma_Y^{(u)}$ far from the measurement points. In the latter case, we assume that the value of the parameter σ_Y present in Eq.(10) may be chosen either as $\sigma_Y^{(u)}$, or as the spatial average of the standard deviation field over the domain Ω. We denote in this section, $\widetilde{Y} = (Y - m_Y)/\sigma_Y$ and $g_k = \lambda_k^{1/2} f_k$. Hence,

$$\widetilde{Y}(\mathbf{x}, \omega) = \sum_{k=1}^{N} \xi_k(\omega) g_k(\mathbf{x}) \tag{23}$$

By replacing Y by $m_Y + \sigma_Y \widetilde{Y}$ in Eq. (6) governing steady groundwater flows, we obtain,

$$\boldsymbol{\nabla}^2 \phi + \boldsymbol{\nabla} m_Y \cdot \boldsymbol{\nabla} \phi = -\sigma_Y \boldsymbol{\nabla} \widetilde{Y} \cdot \boldsymbol{\nabla} \phi - R\, e^{-m_Y - \sigma_Y \widetilde{Y}} \tag{24}$$

where $\widetilde{Y}$ is given by Eq. (23). This equation is of course very difficult to solve. The technique advocated by Ghanem and Spanos [19] consists first in discretizing the spatial operators and obtaining an algebraic (linear) system of equations containing the finite set $\{\xi_n(\theta)\}_{1 \leq n \leq N}$ retained in the truncated KL expansion. The resulting unknown nodal values are then considered as nonlinear functionals of the random variables $\{\xi_n\}_{1 \leq n \leq N}$: if these random variables are Gaussian, such functionals may be expanded in a mean-square convergent Fourier-type series of so-called Wiener-Hermite multivariate polynomials in the ξ_n (referred to as polynomial chaos in [19]). For low values of the ratio I_Y/L, however, the large number of random variables retained in the KL expansion for proper representation of Y precludes the use of Wiener-Hermite expansion.

We resort instead to a perturbation expansion by assuming that σ_Y is a small number. In practical applications, σ_Y can range between 0.65 to 2.3 as reported by Delhomme [13]. We note however that the use of conditional probabilities may significantly reduce the value of the average standard deviation. This approach has been employed in the past [4, 5, 11, 7, 8] and good results have been reported by Dagan [8] for values of σ_Y as large as unity (this will be illustrated in the applications in Section 4). Hence, we expand ϕ in the following form,

$$\phi(\mathbf{x}, \omega) = \phi_0(\mathbf{x}) + \sigma_Y \phi_1(\mathbf{x}, \omega) + \sigma_Y^2 \phi_2(\mathbf{x}, \omega) + \cdots \tag{25}$$

and by identifying terms of same order in σ_Y in (24), we find the sequence of equations, up to order 2,

$$\nabla^2\phi_0 + \nabla m_Y \cdot \nabla\phi_0 = -R\, e^{-m_Y} \tag{26}$$

$$\nabla^2\phi_1 + \nabla m_Y \cdot \nabla\phi_1 = -\nabla\tilde{Y} \cdot \nabla\phi_0 + R\,\tilde{Y} e^{-m_Y} \tag{27}$$

$$\nabla^2\phi_2 + \nabla m_Y \cdot \nabla\phi_2 = -\nabla\tilde{Y} \cdot \nabla\phi_1 - R\,\tilde{Y}^2 e^{-m_Y} \tag{28}$$

We have assumed that the recharge intensity R, as well as the boundary conditions, are deterministic, since it is only the effect of the medium heterogeneity which is of prime interest here.

At the leading order of perturbation, the corresponding BVP (26) governing ϕ_0 is deterministic, and hence, may be readily solved for specified mean field $m_Y(\mathbf{x})$ and recharge $R(\mathbf{x})$, given the boundary conditions,

$$\phi_0 = \phi_b \qquad \text{on } \Gamma_d \tag{29}$$

$$\frac{\partial\phi_0}{\partial n} = \frac{\partial\phi_b}{\partial n} \qquad \text{on } \Gamma_n \tag{30}$$

At the next order of perturbation, the BVP (27) governing $\phi_1(\mathbf{x},\omega)$ is stochastic, but it can be transformed into a sequence of deterministic BVP's by expanding ϕ_1 on the set of random variables $\{\xi_k\}_{k\geq 1}$ used to represent $\tilde{Y}$,

$$\phi_1(\mathbf{x},\omega) = \sum_{k=1}^{\infty} \xi_k(\omega)\, \phi_{1,k}(\mathbf{x}) \tag{31}$$

Indeed, upon substituting this expansion in (27), and using the orthonormality property of the random variables ξ_k, we obtain ($k = 1, 2, \ldots$),

$$\nabla^2\phi_{1,k} + \nabla m_Y \cdot \nabla\phi_{1,k} = -\nabla g_k \cdot \nabla\phi_0 + R\, e^{-m_Y}\, g_k \tag{32}$$

Given ϕ_0 and R, this equation can be solved for each $\phi_{1,k}(\mathbf{x})$ with the corresponding homogeneous boundary conditions,

$$\phi_{1,k} = 0 \qquad \text{on } \Gamma_d \tag{33}$$

$$\frac{\partial\phi_{1,k}}{\partial n} = 0 \qquad \text{on } \Gamma_n \tag{34}$$

If the potential is approximated at this order of approximation, that is,

$$\phi(\mathbf{x},\omega) = \phi_0(\mathbf{x}) + \sigma_Y \sum_{k=1}^{N} \xi_k(\omega)\phi_{1,k}(\mathbf{x}) \tag{35}$$

then, ϕ_0 and $\sigma_Y\phi_1$ represent the mean field m_ϕ and the random fluctuation $\tilde{\phi} = \phi - m_\phi$ about m_ϕ, respectively. In particular, the potential covariance function takes the expression:

$$K_\phi(\mathbf{x},\mathbf{x}') = \mathrm{E}[\tilde{\phi}(\mathbf{x})\tilde{\phi}(\mathbf{x}')] = \sigma_Y^2 \sum_{k=1}^{N} \phi_{1,k}(\mathbf{x})\phi_{1,k}(\mathbf{x}') \tag{36}$$

If ϕ_2 is determined at the next order of perturbation, it will provide corrections to both the mean field m_ϕ and the random fluctuation $\tilde{\phi}$. However, in the present study, we limit computations to a first-order perturbation scheme, that is, to the numerical solution of Eqs. (26) and (32). This is detailed in the following section.

3 THE NUMERICAL MODEL

Equations (26) and (32) governing ϕ_0 and the $\phi_{1,k}$ ($1 \leq k \leq N$), respectively, are Poisson equations which can be transformed into Integral Equations (IE) by applying third Green's identity. Since the only available closed-form expression of Green's function is that associated with the Laplacian operator in the infinite domain (the so-called free-space Green's function), such IE's will involve both boundary and domain integrals. In the numerical model, the latter are transformed into boundary integrals using the Dual Reciprocity (DR) method [16], which requires selecting N_Ω collocation nodes over the domain. Boundary integrals are discretized using N_Γ boundary collocation nodes to describe the variation of geometry, boundary conditions, and unknown functions of the problem. Higher-order boundary elements are used to interpolate between collocation nodes, following a classical Boundary Element Method approach (BEM, [14]). The present numerical model is thus referred to as a DR-BEM model.

3.1 Boundary Element Method

Equation (26) can be transformed into the following equation, for any point $\boldsymbol{\xi}$ in Ω or on Γ,

$$\begin{aligned} c(\boldsymbol{\xi})\phi_o(\boldsymbol{\xi}) &- \int_\Gamma \left\{ G(\boldsymbol{\xi},\mathbf{x})\, \frac{\partial \phi_o}{\partial n}(\mathbf{x}) - \phi_o(\mathbf{x})\, \frac{\partial G}{\partial n}(\boldsymbol{\xi},\mathbf{x}) \right\} d\Gamma(\mathbf{x}) \\ &- \int_\Omega G(\boldsymbol{\xi},\mathbf{x})\, \nabla m_Y(\mathbf{x}) \cdot \nabla \phi_o(\mathbf{x}) d\Omega(\mathbf{x}) \\ &= \int_\Omega G(\boldsymbol{\xi},\mathbf{x})\, R(\mathbf{x})\, e^{-m_Y(\mathbf{x})} d\Omega(\mathbf{x}) \end{aligned} \tag{37}$$

where $G(\boldsymbol{\xi},\mathbf{x})$ is the (logarithmically singular) free-space Green's function of Laplacian operator in two dimensions,

$$G(\boldsymbol{\xi},\mathbf{x}) = \frac{1}{2\pi} \ln |\boldsymbol{\xi} - \mathbf{x}| \tag{38}$$

and $c(\boldsymbol{\xi})$ is a geometric coefficient equal to 1 for points inside the domain ($\boldsymbol{\xi} \in \Omega$) and 1/2 for points on a smooth boundary ($\boldsymbol{\xi} \in \Gamma$).

For Eq. (32), similarly, we have for $k = 1, ..., N$,

$$\begin{aligned} c(\boldsymbol{\xi})\phi_{1,k}(\boldsymbol{\xi}) &- \int_\Gamma \left\{ G(\boldsymbol{\xi},\mathbf{x})\, \frac{\partial \phi_{1,k}}{\partial n}(\mathbf{x}) - \phi_{1,k}(\mathbf{x})\, \frac{\partial G}{\partial n}(\boldsymbol{\xi},\mathbf{x}) \right\} d\Gamma(\mathbf{x}) \\ &- \int_\Omega G(\boldsymbol{\xi},\mathbf{x})\, \nabla m_Y(\mathbf{x}) \cdot \nabla \phi_{1,k}(\mathbf{x}) d\Omega(\mathbf{x}) \\ &= \int_\Omega G(\boldsymbol{\xi},\mathbf{x}) \left\{ \nabla g_k(\mathbf{x}) \cdot \nabla \phi_o(\mathbf{x}) - g_k(\mathbf{x})\, R(\mathbf{x})\, e^{-m_Y(\mathbf{x})} \right\} d\Omega(\mathbf{x}) \end{aligned} \tag{39}$$

Collocation nodes ($\boldsymbol{\xi}_l$; $l = 1, ..., N_\Gamma$) are selected on boundary Γ and Eqs. (37) and (39) are expressed for each of these nodes. The boundary is further divided into M quadratic isoparametric elements, each containing three nodes. Each boundary integral in Eqs. (37) and (39) is thus transformed into a sum of M integrals over each element. Non-singular integrals are computed by a standard Gauss quadrature rule. A kernel transformation is applied to weakly singular integrals which are then integrated by a numerical quadrature, exact for the logarithmic singularity (Grilli *et al.*[15]).

3.2 Simplification for point sources

In applications for which infiltration can be neglected, the recharge R due to the presence of wells may be modeled as the sum of N_s point sources (or sinks) of strength Q_s at $\mathbf{x}_s$, that is, $R(\mathbf{x}) = \sum_{s=1}^{N_s} Q_s \delta(\mathbf{x} - \mathbf{x}_s)$. Then, the corresponding volume integrals of Eqs. (37) and (39) become,

$$\int_\Omega G(\boldsymbol{\xi}, \mathbf{x})\, R(\mathbf{x})\, e^{-m_Y(\mathbf{x})} d\Omega(\mathbf{x}) = \sum_{s=1}^{N_s} Q_s\, G(\boldsymbol{\xi}, \mathbf{x}_s)\, e^{-m_Y(\mathbf{x}_s)} \tag{40}$$

$$\int_\Omega G(\boldsymbol{\xi}, \mathbf{x})\, g_k(\mathbf{x})\, R(\mathbf{x})\, e^{-m_Y(\mathbf{x})} d\Omega(\mathbf{x}) = \sum_{s=1}^{N_s} Q_s\, G(\boldsymbol{\xi}, \mathbf{x}_s)\, g_k(\mathbf{x}_s)\, e^{-m_Y(\mathbf{x}_s)} \tag{41}$$

do not require further treatment.

3.3 Dual Reciprocity BEM

The second and third integrals in Eqs.(37) and (39) are domain integrals. As discussed above, recharge terms may be simplified as in Eq.(40) and (41). Using the DR method [16], the remaining domain integrals can be expressed as boundary integrals of the form,

$$\begin{aligned} \int_\Omega G(\boldsymbol{\xi}, \mathbf{x})\, b(\mathbf{x}) d\Omega(\mathbf{x}) \quad = \quad & -\sum_{j=1}^{N_\Omega} \alpha_j \Big\{ c(\boldsymbol{\xi}) u_j(\boldsymbol{\xi}) \\ & - \int_\Gamma [\, G(\boldsymbol{\xi}, \mathbf{x})\, \frac{\partial u_j}{\partial n}(\mathbf{x}) - u_j(\mathbf{x})\, \frac{\partial G}{\partial n}(\boldsymbol{\xi}, \mathbf{x})\,] d\Gamma(\mathbf{x}) \Big\} \end{aligned} \tag{42}$$

where $b(\mathbf{x})$ denotes part of the right hand side of Poisson's Eqs. (26) and (32) (so-called "body force term"), α_j are coefficients determined by collocation over DR points N_Ω, and $u_j(\mathbf{x})$ are particular solutions of the inhomogeneous equation,

$$\boldsymbol{\nabla}^2 u_j(\mathbf{x}) = \mathcal{F}_j(\mathbf{x}) \qquad (j = 1, ..., N_\Omega) \tag{43}$$

where $\mathcal{F}_j(\mathbf{x})$ denote DR shape functions. Here, we adopt local radial functions defined as,

$$\mathcal{F}_j(\mathbf{x}) = 1 + r_j \qquad , \qquad u_j(\mathbf{x}) = \frac{r_j^2}{4} + \frac{r_j^3}{9} \tag{44}$$

where $r_j = \mid \mathbf{x} - \mathbf{x}_j \mid$.

More specifically, for Eq.(37) governing ϕ_0, we have by definition of shape functions,

$$b(\mathbf{x}) = \boldsymbol{\nabla} m_Y(\mathbf{x}) \cdot \boldsymbol{\nabla} \phi_0(\mathbf{x}) = \sum_{j=1}^{N_\Omega} \alpha_j \, \mathcal{F}_j(\mathbf{x}) \tag{45}$$

Hence, by collocation, the coefficients α_j are obtained according to,

$$\alpha_j = \sum_{v=1}^{N_\Omega} F_{jv}^{-1} \left[\boldsymbol{\nabla} m_Y(\mathbf{x}_v) \cdot \boldsymbol{\nabla} \phi_o(\mathbf{x}_v) \right] \tag{46}$$

where the elements,

$$F_{jv} = \mathcal{F}_j(\mathbf{x}_v) \qquad (j, v = 1, ..., N_\Omega) \tag{47}$$

define the DR collocation matrix, function only of the geometry. Next, we assume a collocation representation of ϕ_0 inside the domain similar to (45) with coefficients β_i, leading to,

$$\boldsymbol{\nabla} \phi_o(\mathbf{x}) = \sum_{i=1}^{N_\Omega} \beta_i \, \boldsymbol{\nabla} \mathcal{F}_i(\mathbf{x}) \tag{48}$$

Combining Eqs. (45) to (48), we have after some algebra,

$$\alpha_j = \sum_{v=1}^{N_\Omega} \sum_{i=1}^{N_\Omega} \sum_{w=1}^{N_\Omega} \left[F_{jv}^{-1} F_{iw}^{-1} F'_{iv} \right] \phi_o(\mathbf{x}_w) = \sum_{w=1}^{N_\Omega} F''_{jw} \phi_o(\mathbf{x}_w) \qquad (j = 1, ..., N_\Omega) \tag{49}$$

where,

$$F''_{jw} = \sum_{v=1}^{N_\Omega} \sum_{i=1}^{N_\Omega} \left[F_{jv}^{-1} F_{iw}^{-1} F'_{iv} \right] \qquad (j, w = 1, ..., N_\Omega) \tag{50}$$

$$F'_{iv} = \boldsymbol{\nabla} m_Y(\mathbf{x}_v) \cdot \boldsymbol{\nabla} \mathcal{F}_i(\mathbf{x}_v) \qquad (i, v = 1, ..., N_\Omega) \tag{51}$$

Finally, using boundary conditions (29), (30) and Eqs. (37), (40), (42), and (49) we have for each BEM and DR collocation node,

$$\begin{aligned}
c(\boldsymbol{\xi}_l)\phi_0(\boldsymbol{\xi}_l) \;&-\; \int_{\Gamma_d} G(\boldsymbol{\xi}_l, \mathbf{x}) \, \frac{\partial \phi_0}{\partial n}(\mathbf{x}) d\Gamma(\mathbf{x}) + \int_{\Gamma_n} \frac{\partial G}{\partial n}(\boldsymbol{\xi}_l, \mathbf{x}) \; \phi_0(\mathbf{x}) d\Gamma(\mathbf{x}) \\
&+\; \sum_{w=1}^{N_\Omega} \phi_0(\mathbf{x}_w) \Bigg\{ \sum_{j=1}^{N_\Omega} F''_{jw} \Bigg\{ c(\boldsymbol{\xi}_l) u_j(\boldsymbol{\xi}_l) \\
&\quad - \int_\Gamma \left[\, G(\boldsymbol{\xi}_l, \mathbf{x}) \, \frac{\partial u_j}{\partial n}(\mathbf{x}) - u_j(\mathbf{x}) \, \frac{\partial G}{\partial n}(\boldsymbol{\xi}_l, \mathbf{x}) \, \right] d\Gamma(\mathbf{x}) \Bigg\} \Bigg\} \\
&=\; \int_{\Gamma_n} G(\boldsymbol{\xi}_l, \mathbf{x}) \, \frac{\partial \phi_b}{\partial n}(\mathbf{x}) d\Gamma(\mathbf{x}) - \int_{\Gamma_d} \frac{\partial G}{\partial n}(\boldsymbol{\xi}_l, \mathbf{x}) \; \phi_b(\mathbf{x}) d\Gamma(\mathbf{x}) \\
&+\; \sum_{s=1}^{N_s} Q_s \, G(\boldsymbol{\xi}_l, \mathbf{x}_s) \, e^{-m_Y(\mathbf{x}_s)} \qquad (l = 1, ..., N_\Gamma + N_\Omega)
\end{aligned} \tag{52}$$

In Eq.(52), unknowns have been moved to the left hand side, i.e. : (i) ϕ_0 at N_Ω DR collocation nodes and at BEM nodes belonging to boundary Γ_n; and (ii) the normal gradient $\partial\phi_0/\partial n$ at BEM nodes belonging to boundary Γ_d (note that there are N_Γ boundary unknowns). Boundary conditions have been moved to the right hand side of Eq.(52) along with known recharge terms Q_s. As mentioned above, by numerical computation of boundary integrals, (52) may be transformed into a linear algebraic system of equations which is solved for the unknowns by a direct elimination method (LU decomposition). Note that, in our applications, DR collocation nodes always include (i.e., overlap with) BEM nodes. This reduces the size of the algebraic system derived from Eq.(52) to $(N_\Omega \times N_\Omega)$. To obtain formally similar matrices in BEM and DR boundary integrals in Eq.(52), the functions u_j and their normal gradient are discretized along the boundary in a manner similar to that of BEM unknowns.

After derivations similar to those for ϕ_0, equation (39) governing $\phi_{1,k}$ $(k = 1, ..., N)$ can be transformed into the following equation, after taking into account the homogeneous boundary conditions (33) and (34),

$$\begin{aligned}
c(\boldsymbol{\xi}_l)\phi_{1,k}(\boldsymbol{\xi}_l) \; &- \; \int_{\Gamma_d} G(\boldsymbol{\xi}_l, \mathbf{x})\, \frac{\partial \phi_{1,k}}{\partial n}(\mathbf{x}) d\Gamma(\mathbf{x}) + \int_{\Gamma_n} \frac{\partial G}{\partial n}(\boldsymbol{\xi}_l, \mathbf{x})\; \phi_{1,k}(\mathbf{x}) d\Gamma(\mathbf{x}) \\
&+ \; \sum_{w=1}^{N_\Omega} \left\{ \sum_{j=1}^{N_\Omega} \left\{ F''_{jw} \phi_{1,k}(\mathbf{x}_w) \; + \; F''^{k}_{jw} \phi_0(\mathbf{x}_w) \right\} \left\{ c(\boldsymbol{\xi}_l) u_j(\boldsymbol{\xi}_l) \right. \right. \\
&\quad \left. \left. - \int_\Gamma [\, G(\boldsymbol{\xi}_l, \mathbf{x})\, \frac{\partial u_j}{\partial n}(\mathbf{x}) - u_j(\mathbf{x})\, \frac{\partial G}{\partial n}(\boldsymbol{\xi}_l, \mathbf{x})\,] d\Gamma(\mathbf{x}) \right\} \right\} \\
&= \; \sum_{s=1}^{N_s} Q_s\, G(\boldsymbol{\xi}_l, \mathbf{x}_s)\, g_k(\mathbf{x}_s)\, e^{-m_Y(\mathbf{x}_s)} \qquad (l = 1, ..., N_\Gamma + N_\Omega)
\end{aligned} \tag{53}$$

with,

$$F''^{k}_{jw} = \sum_{v=1}^{N_\Omega} \sum_{i=1}^{N_\Omega} [\, F^{-1}_{jv} F^{-1}_{iw} F'^{k}_{iv}\,] \qquad (j, w = 1, ..., N_\Omega) \tag{54}$$

$$F'^{k}_{iv} = \boldsymbol{\nabla} g_k(\mathbf{x}_v) \cdot \boldsymbol{\nabla} \mathcal{F}_i(\mathbf{x}_v) \qquad (i, v = 1, ..., N_\Omega) \tag{55}$$

for $k = 1, ..., N$.

4 APPLICATIONS

4.1 Simplifications of DR-BEM equations

Without loss of generality, it will be assumed that, in unconditional modeling, Y has a constant mean over the domain, $m_Y = 0$, and, hence, $Y(\mathbf{x}_i, \omega)$ is a $N(0, \sigma_Y)$ random variable at all locations $\mathbf{x}_i$ of the domain. We will also assume that there are no recharges in the domain, i.e., $Q_s = 0$.

With these hypotheses, DR-BEM equations can be simplified. Eq. (26) for ϕ_0 becomes a Laplace's equation and Eq. (52) now reads,

$$\begin{aligned} c(\boldsymbol{\xi}_l)\phi_0(\boldsymbol{\xi}_l) &- \int_{\Gamma_d} G(\boldsymbol{\xi}_l, \mathrm{x}) \frac{\partial \phi_0}{\partial n}(\mathrm{x}) d\Gamma(\mathrm{x}) + \int_{\Gamma_n} \frac{\partial G}{\partial n}(\boldsymbol{\xi}_l, \mathrm{x}) \; \phi_0(\mathrm{x}) d\Gamma(\mathrm{x}) \\ &= \int_{\Gamma_n} G(\boldsymbol{\xi}_l, \mathrm{x}) \frac{\partial \phi_b}{\partial n}(\mathrm{x}) d\Gamma(\mathrm{x}) - \int_{\Gamma_d} \frac{\partial G}{\partial n}(\boldsymbol{\xi}_l, \mathrm{x}) \; \phi_b(\mathrm{x}) d\Gamma(\mathrm{x}) \end{aligned} \tag{56}$$

for $l = 1, ..., N_\Gamma + N_\Omega$.

Unknowns in Eq. (56) are only located on the boundary and the first N_Γ equations form a linear system yielding boundary nodal values. The last N_Ω equations (minus overlaps of DR and BEM nodes on the boundary) are used to explicitly calculate internal values of ϕ_0 as a function of the boundary solution, needed for the solution of ϕ_1.

With the above simplifications, Eq. (53) for $\phi_{1,k}$ reads, for $k = 1, 2, \ldots N$,

$$\begin{aligned} c(\boldsymbol{\xi}_l)\phi_{1,k}(\boldsymbol{\xi}_l) &- \int_{\Gamma_d} G(\boldsymbol{\xi}_l, \mathrm{x}) \frac{\partial \phi_{1,k}}{\partial n}(\mathrm{x}) d\Gamma(\mathrm{x}) + \int_{\Gamma_n} \frac{\partial G}{\partial n}(\boldsymbol{\xi}_l, \mathrm{x}) \; \phi_{1,k}(\mathrm{x}) d\Gamma(\mathrm{x}) \\ &= - \sum_{w=1}^{N_\Omega} \phi_0(\mathrm{x}_w) \left\{ \sum_{j=1}^{N_\Omega} F_{jw}^{''k} \left\{ c(\boldsymbol{\xi}_l) u_j(\boldsymbol{\xi}_l) \right.\right. \\ &\quad \left.\left. - \int_\Gamma [\; G(\boldsymbol{\xi}_l, \mathrm{x}) \frac{\partial u_j}{\partial n}(\mathrm{x}) - u_j(\mathrm{x}) \frac{\partial G}{\partial n}(\boldsymbol{\xi}_l, \mathrm{x}) \;] \, d\Gamma(\mathrm{x}) \right\} \right\} \end{aligned} \tag{57}$$

for $l = 1, ..., N_\Gamma + N_\Omega$. Hence, the "forcing" for $\phi_{1,k}$ in Eq. (57) only comes from the mean potential value ϕ_0.

4.2 Expression of KL expansion parameters in simple geometry

In the numerical examples, for simplicity, we select a particular random field Y over a rectangular domain, for which closed-form expressions of the KL eigenfunctions and eigenvalues are known. First, consider the scalar homogeneous random process $Y(x)$ defined over the domain $\Omega = [-L, L] \subset \mathbb{R}$, with exponential covariance function $K_Y(x, x') = \sigma_Y^2 \exp\{-|x - x'|/b\}$. After introducing the non-dimensional variable $\tilde{x} = x/L$, and non-dimensional correlation length $\tilde{b} = b/L$, the solutions of the corresponding integral equation on the interval $[-1,\ 1]$ are given by [18],

$$\lambda_k = \frac{2\tilde{b}}{(1 + \tilde{b}^2 \omega_k^2)} \qquad (k \geq 1) \tag{58}$$

where the frequencies ω_k ($k \geq 1$) are the roots of the transcendental equations,

$$\begin{aligned} \cot \omega_k &= \tilde{b}\, \omega_k && \text{for } k \text{ odd} \\ \tan \omega_k &= -\tilde{b}\, \omega_k && \text{for } k \text{ even} \end{aligned} \tag{59}$$

and

$$f_k(\tilde{x}) = \frac{\cos \omega_k \tilde{x}}{\{1+\lambda_k/2\}^{1/2}} \qquad \text{for } k \text{ odd}$$
$$f_k(\tilde{x}) = \frac{\sin \omega_k \tilde{x}}{\{1+\lambda_k/2\}^{1/2}} \qquad \text{for } k \text{ even} \tag{60}$$

It is then possible to extend these results in two dimensions and for the rectangular domain $\Omega = \{(x_1, x_2) \mid \; |x_1| \leq L_1,\, |x_2| \leq L_2\}$; it is easily shown that a separable covariance function, i.e., $K_Y(x_1, x_2; x_1', x_2') = K_1(x_1, x_1')K_2(x_2, x_2')$, leads to separable eigenfunctions, i.e. of the form $f_{m,n}(x_1, x_2) = f_m^{(1)}(x_1) f_n^{(2)}(x_2)$ with corresponding eigenvalues $\lambda_{m,n} = \lambda_m^{(1)}\lambda_n^{(2)}$, where the sets $\{f_n^{(\alpha)}\}$ and $\{\lambda_n^{(\alpha)}\}$ correspond to kernel K_α $(\alpha = 1, 2)$.

Hence, the random field $\tilde{Y} = (Y - m_Y)/\sigma_Y$ admits the following representation from Eq. (23),

$$\tilde{Y}(\mathbf{x}, \omega) = \sum_{n=1}^{N} \xi_n(\omega)\, \lambda_n^{1/2}\, f_n(\mathbf{x}) = \sum_{k=1}^{K}\sum_{l=1}^{L} \xi_{k,l}(\omega)\, \{\lambda_k^{(1)}\lambda_l^{(2)}\}^{1/2}\, f_k^{(1)}(x_1) f_l^{(2)}(x_2) \tag{61}$$

A few numerical results are useful at this point to illustrate the qualitative and quantitative properties of this expansion. First, as seen in Fig. 2(a), for each value of $\tilde{b} = 0.1$, 1 and 10, the spectrum of eigenvalue tends to zero, thereby indicating convergence of the expansion in the one-dimensional case. However, as the correlation scale $\tilde{b}$ tends to zero, this spectrum tends to flatten out and, hence, the convergence of the KL expansion tends to become slower. Fig. 2(b) also shows that the eigenfunctions tend to become increasingly more oscillatory as the order k increases, and the high-order eigenfunctions determine the small scale structure of the realizations of Y. The case $\tilde{b} = b/L = 0.1$ is more typical of porous media, and the slow convergence of the expansion implies that more terms will be needed to achieve a preselected accuracy of the computations. Furthermore, in the numerical model, more internal DR points will be needed in Eq. (57), to accurately capture the oscillations of eigenfunctions corresponding to large orders k. Fig. 3 shows an example of a two-dimensional realization of a Gaussian homogeneous random field $Y(x_1, x_2, \omega)$ with covariance $K_Y(r_1, r_2) = \sigma_Y^2 \exp\{-|r_1|/b_1 - |r_2|/b_2\}$, for $b_1/L_1 = b_2/L_2 = 0.1$, where $N = K \times L = 100$ terms have been used to represent Y. This figure gives an idea of the difficult task of performing Monte Carlo simulations to solve for the flow, given each realization of the medium characterized by a small ratio I_Y/L. A grid size smaller than the correlation scale I_Y must be used to resolve the small scale structure of the medium. The numerical problems (26) and (32) involve similar equations, however the heterogeneous character of each realization $Y(\mathbf{x}, \omega_i)$ has now been replaced by the much smoother and regular behavior of the mean field m_Y and the KL eigenfunctions.

The approach described in Section 2.2 for conditional modeling of the log-transmissivity is illustrated in Fig. 4(ab), where the transmissivity is conditioned on values obtained at five locations. This figure shows the conditional mean $m_Y^c(\mathbf{x})$ and standard deviation $\sigma_Y^{(c)}(\mathbf{x})$ computed by : (i) KL expansion $\sum_{k=1}^{N} \lambda_k^{(c)}(f_k^{(c)}(\mathbf{x}))^2$, where the conditional eigenvalues/functions are computed based on Eq. (21); and (ii) direct numerical resolution of the exact Eqs. (14) and (15). Good agreement is seen, but we note that the convergence of series of the type $f^{(c)}(\mathbf{x}) = \sum_{k=1}^{\infty} \alpha_k^{(c)} f_k(\mathbf{x})$ becomes slower as the ratio I_Y/L becomes smaller, and hence it may become more efficient to solve the conditional eigenproblem by a direct numerical method. We nevertheless adopt this scheme for our last example in Section 4.6 (problem 3).

4.3 Comparison of DR-BEM with Monte-Carlo method

The DR-BEM numerical method is applied on three case problems with a square geometry $\Omega = \{(x_1, x_2) \mid |x_1| \leq L,\ |x_2| \leq L\}$. A constant head gradient $(\phi_{b1} - \phi_{b2})$ is specified on the boundary Γ_d. In terms of non-dimensional variables, $\tilde{\phi} = \phi/(\phi_{b1} - \phi_{b2})$ and $(\tilde{x}_1, \tilde{x}_2) = (x_1/L, x_2/L)$, the governing equations and boundary conditions are given by (dropping the tilde notation from thereon),

$$\nabla^2\phi + \nabla Y \cdot \nabla\phi = 0, \quad \text{in} \quad -1 < x_1, x_2 < 1 \tag{62}$$

$$\phi = 0, \quad \text{on } \Gamma_{d1}, \qquad \phi = 1, \quad \text{on } \Gamma_{d2} \tag{63}$$

$$\frac{\partial\phi}{\partial n} = 0 \quad \text{on } \Gamma_n. \tag{64}$$

The spatial correlation of Y is assumed to be given by Eq. (12), with corresponding eigenvalues and eigenfunctions in the KL expansion given by Eqs. (58) to (60).

Our DR-BEM scheme will be validated by comparing results with those obtained by Monte-Carlo (MC) simulations whereby the governing equation (6), with boundary conditions (7) and (8), is solved using an Alternate Direction of Integration (ADI) finite difference method, for a large number of realizations of the random log-transmissivity Y. For an efficient generation of realizations of Y over domain Ω, the KL expansion (10) is used in which a corresponding number of independent realizations of the Gaussian random variables $\xi_k(\omega)$ are generated. Each realization of the potential ϕ is calculated over the domain corresponding to each realization of Y. The potential mean m_ϕ and standard deviation σ_ϕ fields are then calculated by ensemble averaging. Examples of realizations of the potential and of its statistics are given in the following sections.

For each DR-BEM problem, we must check for convergence under increased number of terms in KL expansion of Y and under spatial grid refinement, that is, under increased number $N_\Gamma + N_\Omega$ of nodal points on the boundary and inside the domain. For MC simulations, convergence must be checked under spatial grid refinement and increased number of computed realizations (statistical convergence).

4.4 Test problem 1

Our first application corresponds to the simple square geometry and boundary conditions sketched in Fig. 5, which essentially represents a uniform average horizontal flow between two impermeable plates in a random porous medium. Computations are made with the present DR-BEM approach, for various values of the parameters of both the physical problem and the numerical method. Results are compared with those obtained following the MC approach.

As shown in Fig. 5, the domain boundary corresponds to $x_1 = \pm 1$ and $x_2 = \pm 1$. We impose $\phi_b = 0$ on $x_1 = -1$ and $\phi_b = 1$ on $x_1 = +1$. The lower and upper boundaries $x_2 = \pm 1$ are impermeable and $q = \partial\phi/\partial n = 0$ is imposed. The log-transmissivity standard deviation is fixed to

$\sigma_Y = 1$, and correlation lengths are set equal in both directions, successively to $b = b_1 = b_2 = 0.1$, 0.2 and 1.0. Note that the large value adopted here for σ_Y will make this a very demanding test for validating our DR-BEM scheme, since the perturbation expansion assumed for ϕ requires the assumption $\sigma_Y \ll 1$.

Results of both the MC and the DR-BEM methods for the mean potential yield the linear variation $m_\phi = (x_1 + 1)/2$ expected for the deterministic homogeneous problem (i.e. $Y =$ Constant), irrespective of the values of σ_Y and b. Hence, no graphical representation of m_ϕ is shown. Fig. 6 presents results for the potential standard deviation σ_ϕ obtained with the DR-BEM approach and Fig. 7 gives the same results obtained with a MC approach, for a large number of realizations ensuring satisfactory convergence of the results. As the value of b is reduced, an increasing number of KL terms is used in the DR-BEM method. The same number of KL terms is used for the representation of Y in corresponding MC simulations.

In the DR-BEM results presented in Fig. 6, the finer spatial discretization, with a 0.1x0.1 grid (i.e., $N_\Omega = 441$ nodes and $N_\Gamma = 81$ nodes), is used for sake of accuracy of the spatial representation, but rather identical results can be obtained, particularly for the larger values of b, with a much coarser spatial discretization (down to $N_\Omega = 121$ nodes and $N_\Gamma = 41$ nodes), and thus a much reduced computational effort.

A quick visual comparison of DR-BEM and MC results in Figs. 6 and 7 shows the good agreement between both approaches and Fig. 8 confirms these observations, showing the variation of σ_ϕ obtained along the x_1-axis with both methods. For both schemes, the head standard deviation σ_ϕ tends to decrease with the correlation length b, and for small b, a boundary layer profile is observed, that is, a constant value is reached inside Ω, with a fast variation near the boundary Γ_d.

Overall, for the three b values, the DR-BEM method yields results of σ_ϕ within 15% of those obtained with the MC simulations. Results with the DR-BEM method, however, are obtained with a much smaller computational effort than required with the MC simulations (CPU times are 10-100 times less depending on discretizations). Besides, MC results do not offer the same degree of smoothness as DR-BEM results.

4.5 Test problem 2

In this second example, the geometry and modeling of Y are kept identical to those of case 1. Boundary conditions, however, are changed, as shown in Fig. 9, to the following,

$$\begin{aligned} \phi_b = 0, \quad \text{on} \quad \{x_1 = -1,\ -1 \le x_2 \le -1 + r\} \bigcup \{x_2 = -1,\ -1 \le x_1 \le -1 + r\} \\ \phi_b = 1, \quad \text{on} \quad \{x_1 = 1,\ -1 \le x_2 \le 1 - r\} \bigcup \{x_2 = 1,\ -1 \le x_1 \le 1 - r\} \\ \frac{\partial \phi}{\partial n} = 0, \quad \text{elsewhere} \end{aligned} \tag{65}$$

We fix $r = 0.1$, $\sigma_Y = 1$, and, successively, $b = b_1 = b_2 = 0.1, 0.2$, and 1. We proceed as in case 1 and similar results are shown for σ_ϕ in Figs. 10, 11 and 12 (which here compares σ_ϕ along the diagonal, $x_1 = x_2$). Results for the mean field m_ϕ (not shown here) agree very well between the two numerical schemes, and are found independent of the values of b and σ_Y. DR-BEM and MC results for the standard deviation σ_ϕ are again quite similar, both qualitatively and quantitatively.

Again, in both the DR-BEM and MC results, the standard deviation σ_ϕ tends to decrease and homogenize as $b \to 0$. Overall, for the three b values, the DR-BEM method yields results of σ_ϕ within 15% to 20% of those obtained with the MC simulations.

4.6 Test problem 3

In this last example, the boundary conditions are taken as in case 2, but the modeling of Y is modified by conditioning its value at five locations : $O(0,0)$, $A(-\frac{1}{2},\frac{1}{2})$, $B(\frac{1}{2},\frac{1}{2})$, $C(-\frac{1}{2},-\frac{1}{2})$, and $D(\frac{1}{2},-\frac{1}{2})$ (see Fig. 13 for the values of Y adopted at these points). The following parameter values are selected : $\sigma_Y = 1$, $b = 0.2$, and $r = 0.2$.

Conditional eigenfunctions and eigenvalues of the KL expansion are obtained as described in Section 4.2. In this situation, the mean m_Y^c of log-transmissivity is no longer constant. According to first-order perturbation, the mean field $m_\phi = \phi_0$ is obtained as if the medium was characterized by a log-transmissivity equal to the conditional mean m_Y^c. Hence, even with only five points, there is a marked difference in the mean response between conditional and corresponding unconditional cases. This is shown in Fig. 14.

Figs. 15 and 16 show that, again, both DR-BEM and MC results for σ_ϕ agree quite well. The expected reduction in the standard deviation σ_ϕ due to conditioning is felt over most of the domain but is small in absolute value, about 10%, due to the small number of conditioning points used in this example.

Despite the small reduction in σ_ϕ, however, the standard deviation of the specific discharge vector $\mathbf{q} = -T\boldsymbol{\nabla}\phi$ would be significantly affected by the conditioning, due to the logarithmic transformation, $Y = \ln T$. This, in turn, would also significantly affect predictions of solute transport that could be done based on calculated flows. We intend in the future to illustrate these aspects of the problem using more realistic test cases of conditional modeling.

5 CONCLUDING REMARKS

A DR-BEM numerical method for calculating groundwater flows in random porous media, based on a KL perturbation expansion assuming small σ_Y, was presented and validated, using three test cases, by comparing results with Monte Carlo simulations. In the test cases, a large value $\sigma_Y = 1$ is used which may stretch the validity of the perturbation scheme. Overall, results from both methods are found realistic but DR-BEM results overestimate MC results by 15-20%. This could be due to the large finite value of σ_Y. DR-BEM results, however, are much more computationally efficient than MC results.

More specifically :

1. Numerical results were presented for both mean and standard deviations, but other hydraulic head statistics may be computed from the expansion

$$\phi(\mathbf{x},\omega) = \phi_0(\mathbf{x}) + \sigma_Y \sum_{k=1}^{N} \xi_k(\omega)\phi_{1,k}(\mathbf{x}) \tag{66}$$

This expression may prove useful in future work, to predict statistical results pertaining to solute transport.

2. Test cases were limited to a simple square geometry, with a covariance function that admits closed-form KL expansion eigenvalues and eigenfunctions. However, the numerical scheme can be easily extended to more general geometry and transmissivity covariance function.

3. In light of expansion (66), the response is Gaussian, a result which tends to be supported by field measurements of hydraulic heads. Non-Gaussian deviations can be accounted for in a second-order perturbation scheme, albeit at a much higher computational cost. But note that second-order terms will only contribute to larger errors of the head standard deviation σ_ϕ.

4. A more appropriate asymptotic analysis of the flow equation (6) should be conducted, not in the limit $\sigma_Y \to 0$ but rather in the limit $I_Y/L \to 0$, keeping σ_Y of order 1. Indeed, our perturbation scheme is strictly valid for $\sigma_Y \ll 1$ and, moreover, in the limit $I_Y/L \to 0$, KL expansions become divergent. Asymptotic results in the limit $I_Y/L \to 0$ can be obtained by the method of *homogenization*, which attempts to derive an homogenized equation for the mean fields, with *effective* parameters (here, effective hydraulic transmissivity), for statistically homogeneous ergodic media. But no information is usually obtained for the statistics of the random fluctuations, which has been our goal in the present work. It would thus be beneficial to derive a truly stochastic homogenization, yielding more than effective properties and mean flows.

References

[1] Bear, J., *Dynamics of Fluids in Porous Media*, New York: Elsevier, 1972.

[2] Freeze, R. A., A Stochastic Conceptual Analysis of One-Dimensional Groundwater in Nonuniform Homogeneous Media, *Water Resour. Res.*, **11** (5), 725-741, 1975.

[3] Smith, L., and Freeze, R. A., Stochastic analysis of steady-state groundwater flow in a bounded domain. 2. Two-dimensional simulations. *Water Resour. Res.*, **15** (6), 1543-1559, 1979.

[4] Bakr, A. A., Gelhar, L. W., Gutjahr, A. L., MacMillan, J. R., Stochastic analysis of spatial variability of subsurface flows. 1. Comparison of one- and three-dimensional flows, *Water Resour. Res.*, **14** (2), 263-271, 1978.

[5] Gutjahr, A. L., Gelhar, L. W., Bakr, A. A., MacMillan, J. R., Stochastic analysis of spatial variability of subsurface flows. 2. Evaluation and application. *Water Resour. Res.*, **14**, 953-959, 1978.

[6] Dagan, G., Models of Groundwater Flow in Statistically Homogeneous Porous Formations, *Water Resour. Res.*, **15** (1), 47-63, 1979.

[7] Dagan, G., Stochastic modeling of groundwater flow by unconditional and conditional probabilities. 1. Conditional simulation and the direct problem. *Water Resour. Res.*, **18** (4), 813-833, 1982.

[8] Dagan, G., A note on the higher-order corrections of the head covariances in steady aquifer flow.*Water Resour. Res.*, **21**, 573-578, 1985.

[9] Dagan, G., Theory of solute transport by groundwater, *Ann. Rev. Fluid Mech.*, **19**, 183-215, 1987.

[10] Dagan, G., *Flow and Transport in Porous Formations*. Springer-Verlag, 1989.

[11] Sagar, B., Galerkin finite element procedure for analyzing flow through random media. *Water Resour. Res.*, **14**(6), 1035-1044, 1978.

[12] Delhomme, J. P., Kriging in the hydrosciences. *Adv. Water Resour.*, **1**(5), 251-266, 1978.

[13] Delhomme, J. P., Spatial variability and uncertainty in groundwater flow parameters: A geostatistical approach. *Water Resour. Res.*, **15**(2), 269-280, 1979.

[14] Brebbia, C.A., *The Boundary Element Method for Engineers.* John Wiley and Sons, 1978.

[15] Grilli, S., Skourup, J. and I.A., Svendsen, An efficient boundary element method for nonlinear water waves. *Engng. Analysis with Boundary Elements* **6** (2), 97-107, 1989.

[16] Partridge, P.W., Brebbia, C.A. and Wrobel, L.C., *The Dual Reciprocity Boundary Element Method.* Computational Mechanics Publication, Elsevier, 1992.

[17] Courant, R., and Hilbert, D., *Methods of Mathematical Physics*, Vol. 1, New York : Interscience, 1953.

[18] Papoulis, A., *Probability, Random Variables, and Stochastic Processes*, New York: McGraw-Hill, 1965.

[19] Ghanem, R. G., and Spanos, P. D., *Stochastic Finite Elements : a Spectral Approach*, New York : Springer-Verlag, 1991.

[20] Beliaev, A.Y., and Kozlov, S.M. , Darcy equation for random porous media, *Communications on Pure & Applied Mathematics*, **49** (1), 1-34, 1996.

List of figures:

Fig.1: Sketch of porous medium with boundary conditions on Γ_d, where $\phi = \phi_b$, and on Γ_n, where $q = \partial\phi/\partial n$.

Fig.2: (a) The spectrum of eigenvalues for $K_Y(\widetilde{x}, \widetilde{x}') = \exp\{-|\widetilde{x} - \widetilde{x}'|/\widetilde{b}\}$, $(-1 \leq \widetilde{x} \leq 1)$ for $\widetilde{b} = 0.1,\ 1$, and 10. (b) The first five corresponding eigenfunctions for $\widetilde{b} = 1$.

Fig.3: A realization of a Gaussian field $Y(\widetilde{x}_1, \widetilde{x}_2, \omega)$ over the domain $-1 \leq \widetilde{x}_1, \widetilde{x}_2; \leq 1$, with covariance $K_Y(r_1, r_2) = \sigma_Y^2 \exp\{-|r_1|/b_1 - |r_2|/b_2\}$, for $\widetilde{b}_1 = b_1/L_1 = 0.1$ and $\widetilde{b}_2 = b_2/L_2 = 0.1$, with $m_Y = 0$ and $\sigma_Y = 1$. $N = 10$ KL expansion terms are used in each direction.

Fig.4: KL representation of Y (with $L = 25$ unconditional KL functions chosen to solve Eq. (21)) conditioned at the five points : $O(0,0)$ $(Y(O) = 0)$, $A(-\frac{1}{2}, \frac{1}{2})$ $(Y(A) = 0.5)$, $B(\frac{1}{2}, \frac{1}{2})$ $(Y(B) = -1)$, $C(-\frac{1}{2}, -\frac{1}{2})$ $(Y(C) = 1)$, $D(\frac{1}{2}, -\frac{1}{2})$ $(Y(D) = 0)$. The unconditional covariance function (12) is chosen with parameters $\widetilde{b}_1 = \widetilde{b}_2 = 0.5$ and $\sigma_Y = 1$. (a) mean field $m_Y^c(\mathbf{x})$; (b) standard deviation $\sigma_Y^{(c)}(\mathbf{x})$; (c) σ_Y by exact numerical solution of Eqs. (13), (14), (15).

Fig.5: Sketch of computational domain and boundary conditions for case 1: $\phi = 0$ on $x_1 = -1$, $\phi = 1$ on $x_1 = 1$, $q = 0$ on $x_2 = \pm 1$ (with $q = \partial\phi/\partial n$).

Fig.6: DR-BEM results for σ_ϕ, case 1 : (a) $b = 0.1$, 15x15 KL terms; (b) $b = 0.2$, 9x9 KL terms; (c) $b = 1.0$, 6x6 KL terms.

Fig.7: MC results for σ_ϕ, case 1. Same cases as in Figure 6 with number of realizations: (a) 5,000; (b) 2,000; (c) 1,000, and spatial step size $\Delta_1 = \Delta_2$: (a) 0.02 (100x100 nodal points), (b) 0.025 (80x80 nodal points) , (c) 0.04 (50x50 nodal points)

Fig.8: Comparison between σ_ϕ calculated by DR-BEM (continuous lines) and MC (dotted lines) on axis $x_2 = 0$, for cases of Figs. 6 and 7.

Fig.9: Sketch of computational domain and boundary conditions for case 2 ($r = 0.1$).

Fig.10: DR-BEM results for σ_ϕ, case 2: (a) $b = 0.1$, 15x15 KL terms; (b) $b = 0.2$, 9x9 KL terms; (c) $b = 1.0$, 6x6 KL terms.

Fig.11: MC results for σ_ϕ, case 2. Same cases as in Fig.10 with number of realizations: (a) 5,000; (b) 3000; (c) 2000 , and spatial step size $\Delta_1 = \Delta_2$: (a) 0.02 (100x100 nodal points), (b) 0.025 (80x80 nodal points) , (c) 0.04 (50x50 nodal points).

Fig.12: Comparison between between σ_ϕ calculated by DR-BEM (continuous lines) and MC (dotted lines) on line $x_2 = x_1$, for cases of Figs. 10 and 11.

Fig.13: Sketch of computational domain and boundary conditions for case 3 ($r = 0.2$). The log-transmissivity is conditioned at the points : $O(0,0)$, $A(-\frac{1}{2}, \frac{1}{2})$, $B(\frac{1}{2}, \frac{1}{2})$, $C(-\frac{1}{2}, -\frac{1}{2})$, $D(\frac{1}{2}, -\frac{1}{2})$, where Y is assigned the values $0, 0.5, -1, 1$ and 0, respectively. The KL representation of Y is done by solving Eq. (21) with $L =$ 10x10 unconditional KL functions to assure proper convergence of the expansion. The conditioning is based on the covariance kernel (12), with $\sigma_Y = 1$ and $b_1 = b_2 = 0.2$.

Fig.14: Mean field m_ϕ on line $x_1 = x_2$ with conditioning (continuous line) and without conditioning (dotted lined). Results of DR-BEM and MC are in quantitative agreement.

Fig.15: DR-BEM results for case 3 corresponding to the geometry of Fig.13 with $r = 0.2$: (a) mean field m_ϕ, (b) standard deviation σ_ϕ.

Fig.16: MC results, case 3 with parameters of Fig. 13 with 5000 realizations and grid size $\Delta_1 = \Delta_2 = 0.0125$ (80x80 nodal points) : (a) mean field m_ϕ, (b) standard deviation σ_ϕ.

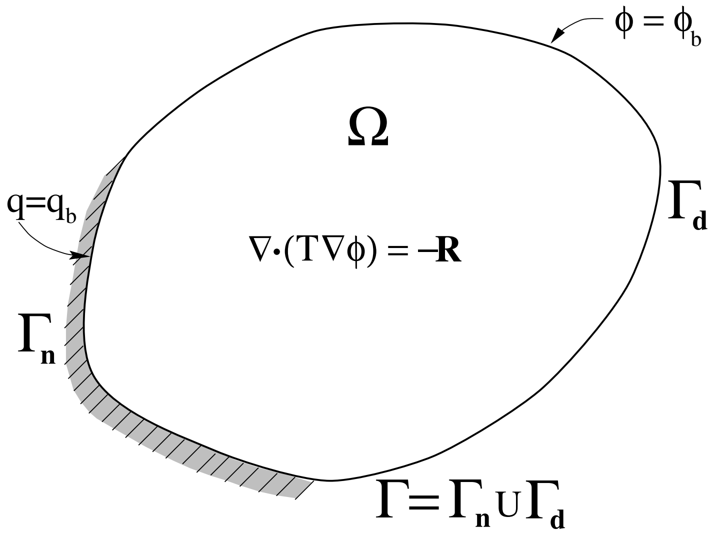
$\phi = \phi_b$
Ω
$q=q_b$
Γ_d
$\nabla\cdot(T\nabla\phi) = -\mathbf{R}$
Γ_n
$\Gamma = \Gamma_n \cup \Gamma_d$

Figure 1

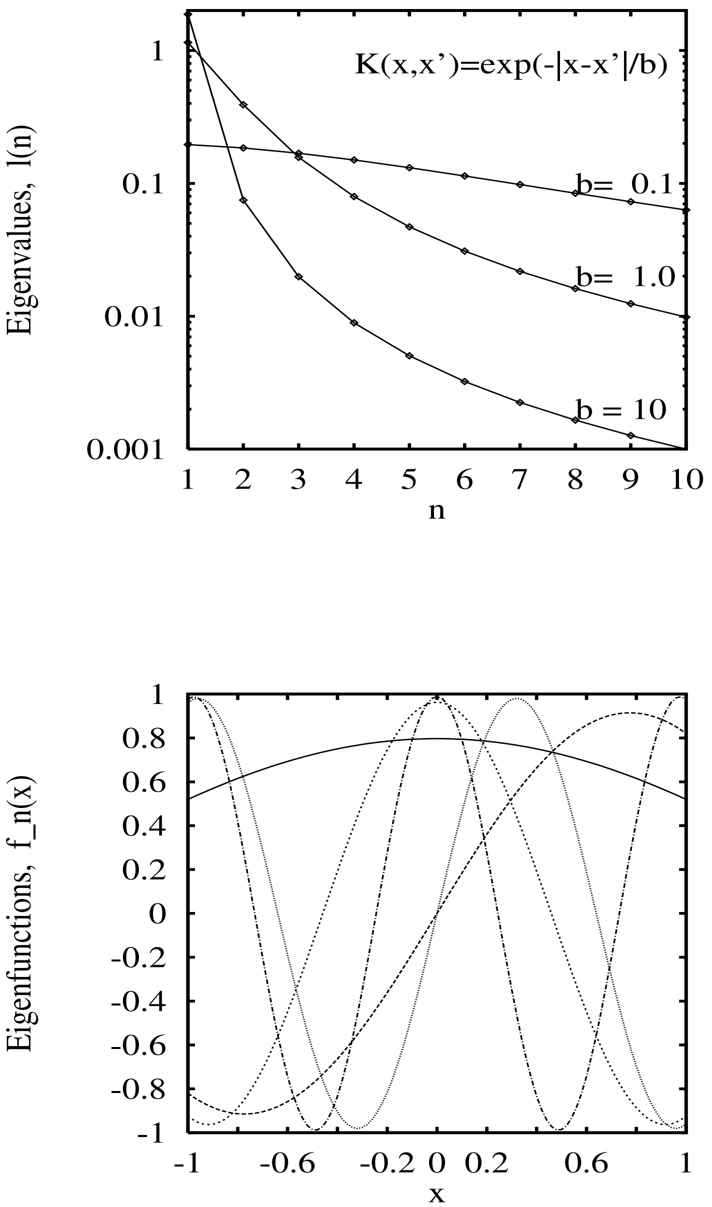

K(x,x')=exp(-|x-x'|/b)
Eigenvalues, l(n)
b= 0.1
b= 1.0
b = 10
1
0.1
0.01
0.001
1 2 3 4 5 6 7 8 9 10
n
Eigenfunctions, f_n(x)
1
0.8
0.6
0.4
0.2
0
-0.2
-0.4
-0.6
-0.8
-1
-1 -0.6 -0.2 0 0.2 0.6 1
x

Figure 2

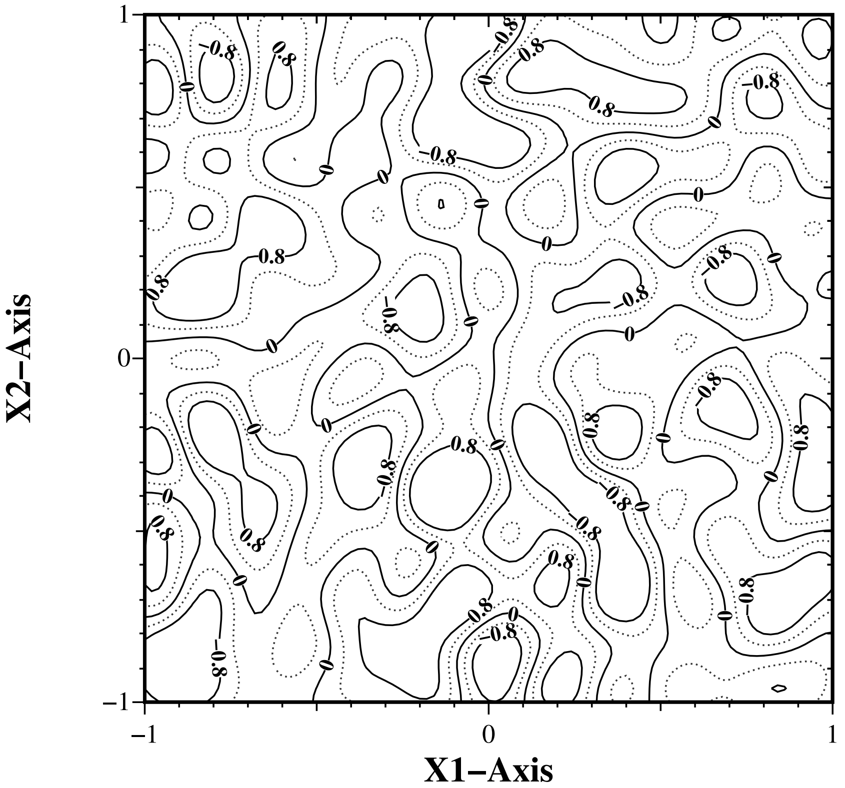

Figure 3

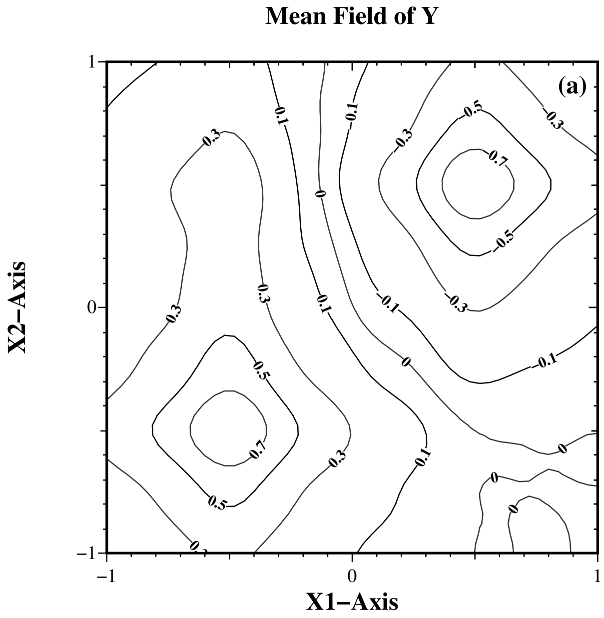

Mean Field of Y
(a)
X2−Axis
X1−Axis
1
0
−1
−1
0
1

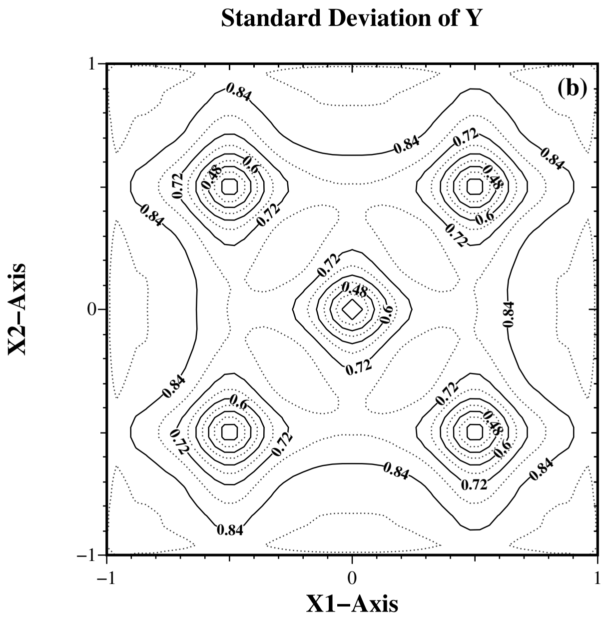

Standard Deviation of Y
(b)
X2−Axis
X1−Axis
1
0
−1
−1
0
1

Figure 4

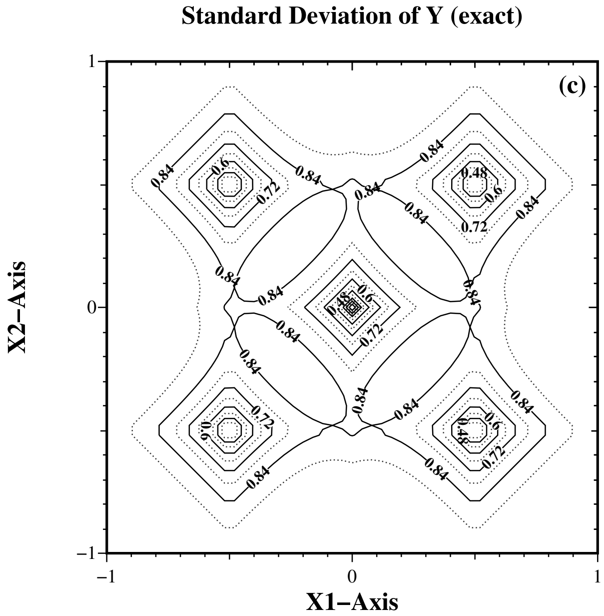

Figure 4 (cont.)

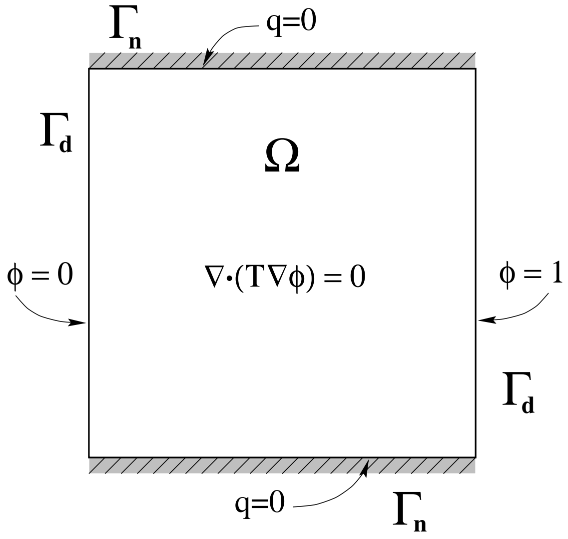

Figure 5

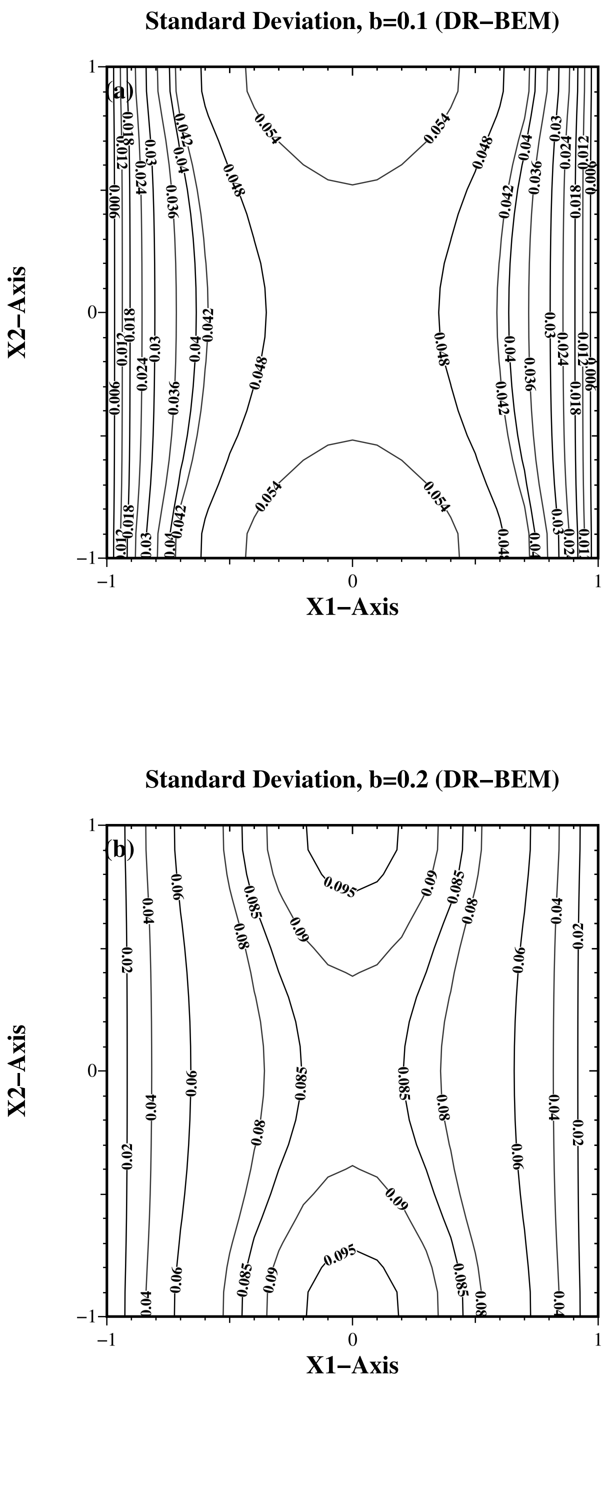

Standard Deviation, b=0.1 (DR−BEM)
(a)
X2−Axis
X1−Axis
0.006
0.012
0.018
0.024
0.03
0.036
0.04
0.042
0.048
0.054
Standard Deviation, b=0.2 (DR−BEM)
(b)
X2−Axis
X1−Axis
0.02
0.04
0.06
0.08
0.085
0.09
0.095

Figure 6

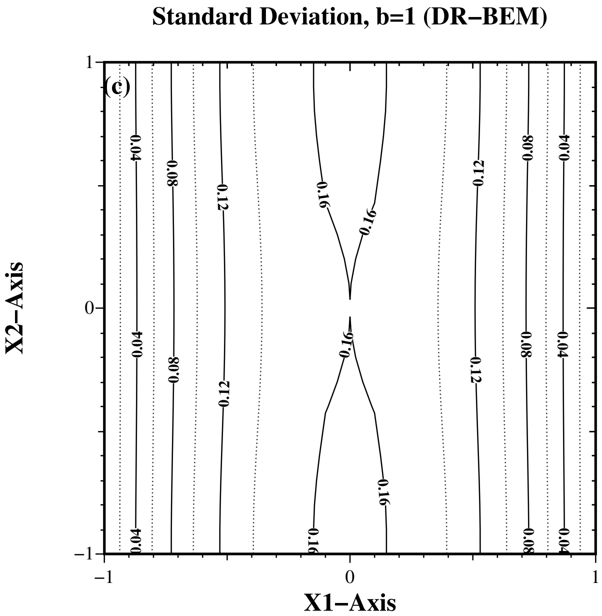

Figure 6 (cont.)

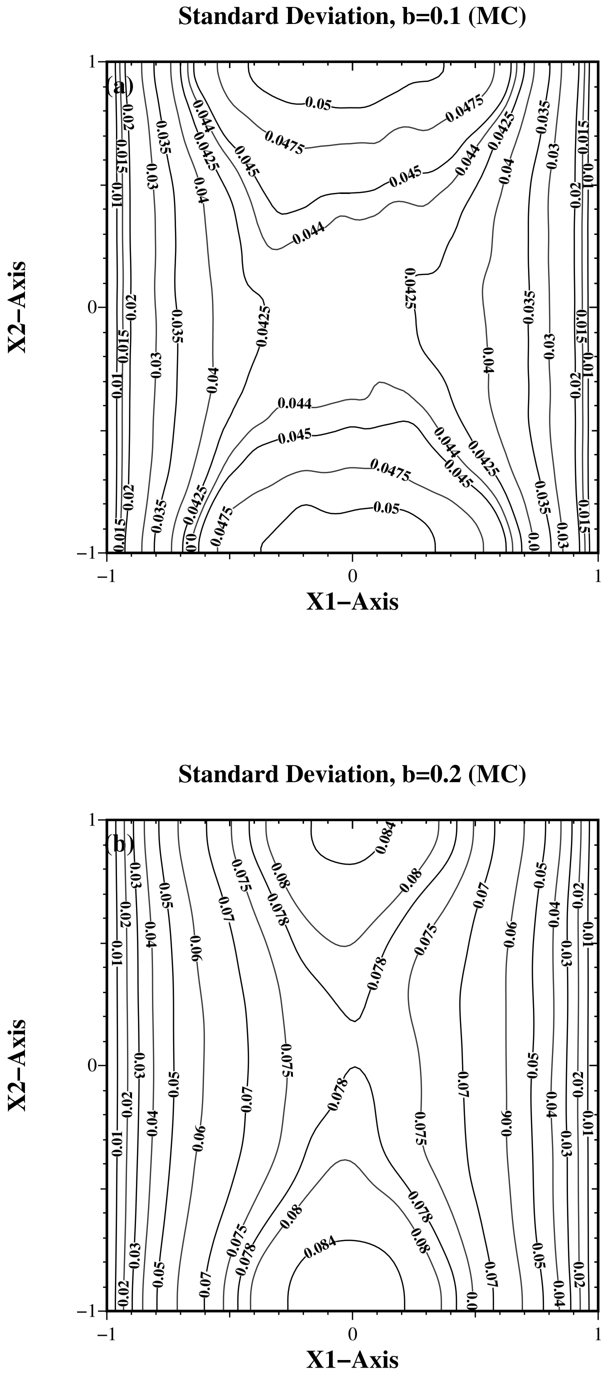
Standard Deviation, b=0.1 (MC)
(a)
X2−Axis
X1−Axis
Standard Deviation, b=0.2 (MC)
(b)
X2−Axis
X1−Axis

Figure 7

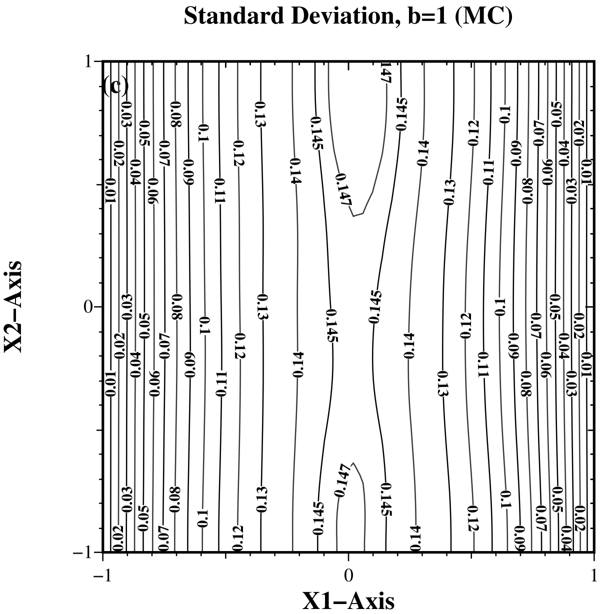

Figure 7 (cont.)

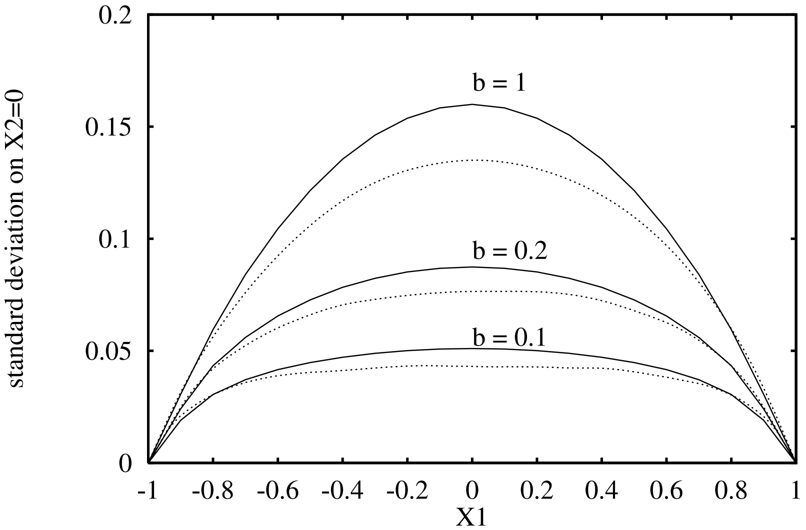

Figure 8

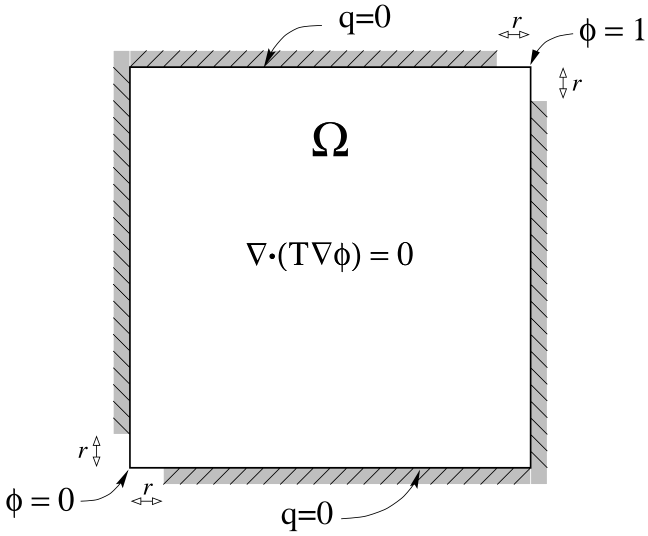

Figure 9

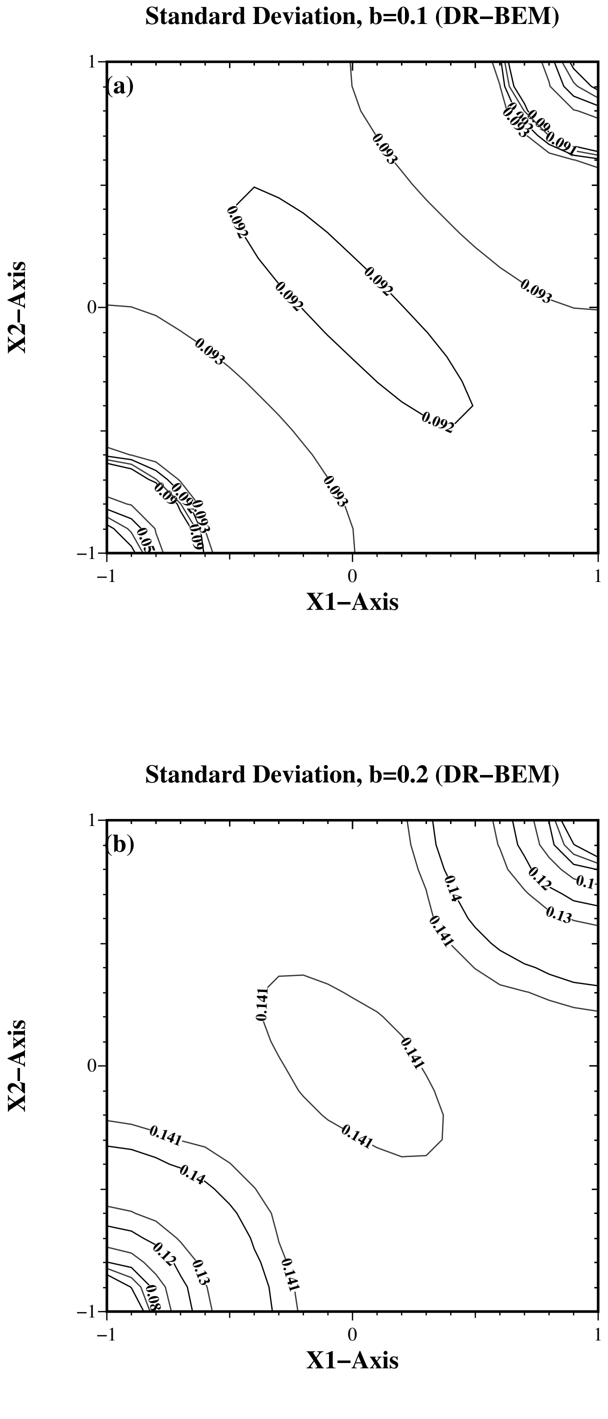
Standard Deviation, b=0.1 (DR−BEM)
(a)
0.093
0.092
0.092
0.092
0.092
0.093
0.093
0.093
X2−Axis
X1−Axis
−1
0
1
Standard Deviation, b=0.2 (DR−BEM)
(b)
0.14
0.141
0.12
0.13
0.141
0.141
0.141
0.141
0.14
0.12
0.13
0.141
0.08
X2−Axis
X1−Axis
−1
0
1

Figure 10

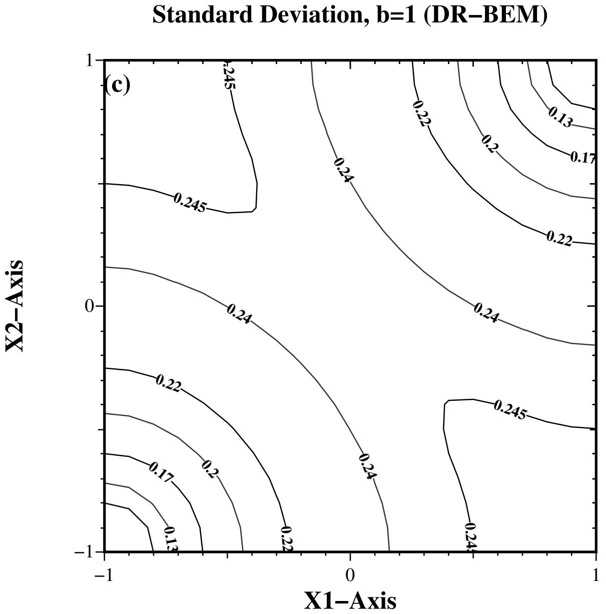

Figure 10 (cont.)

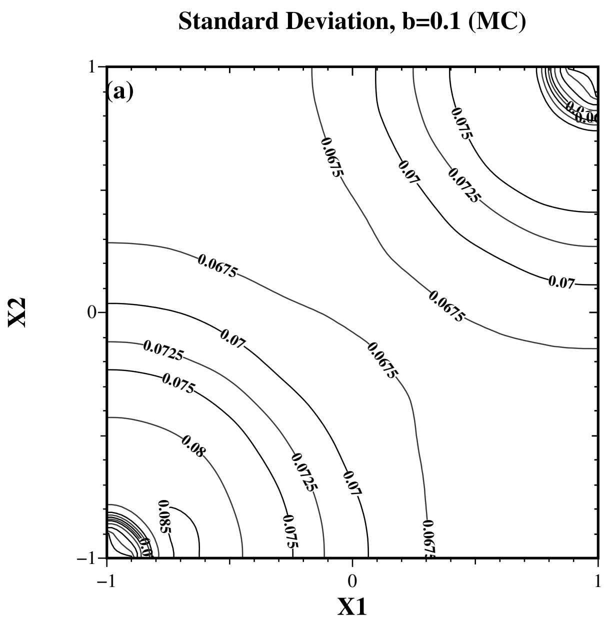

Standard Deviation, b=0.1 (MC)
(a)
X2
X1

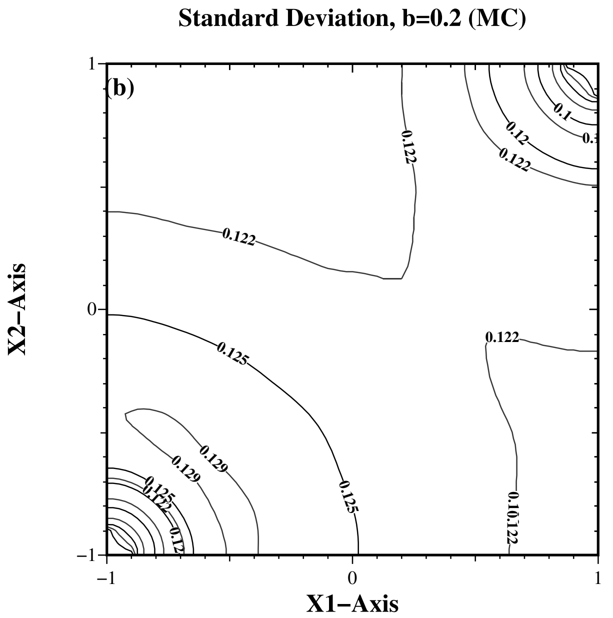

Standard Deviation, b=0.2 (MC)
(b)
X2−Axis
X1−Axis

Figure 11

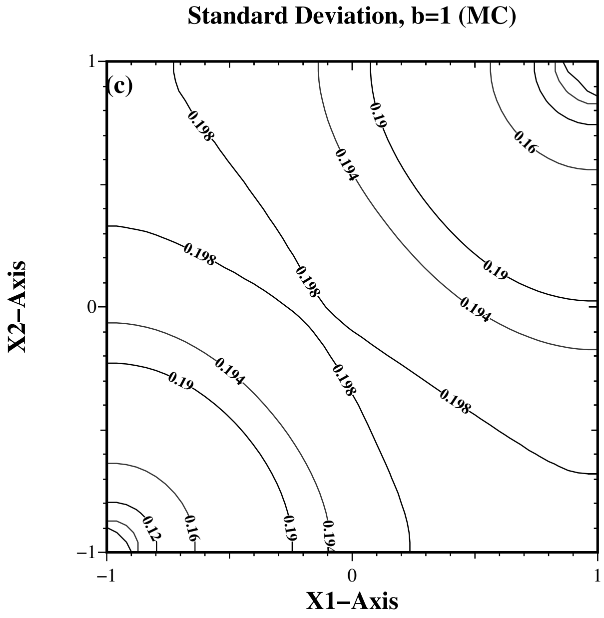

Figure 11 (cont.)

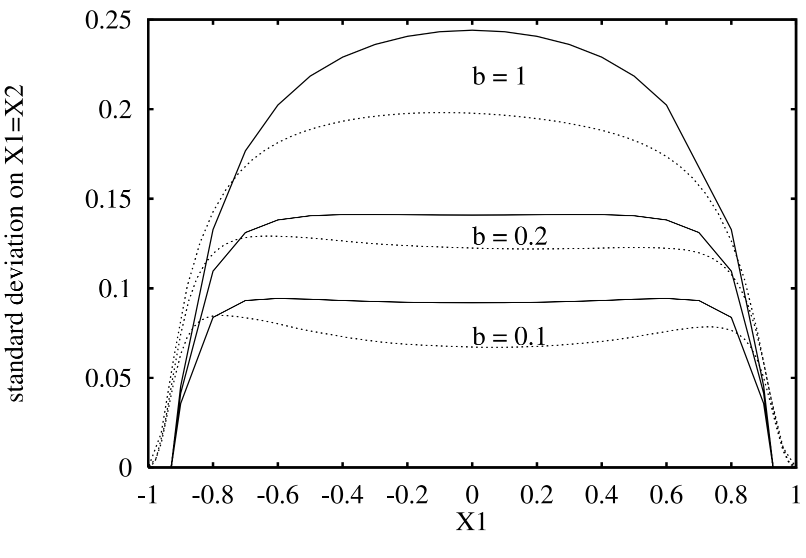

Figure 12

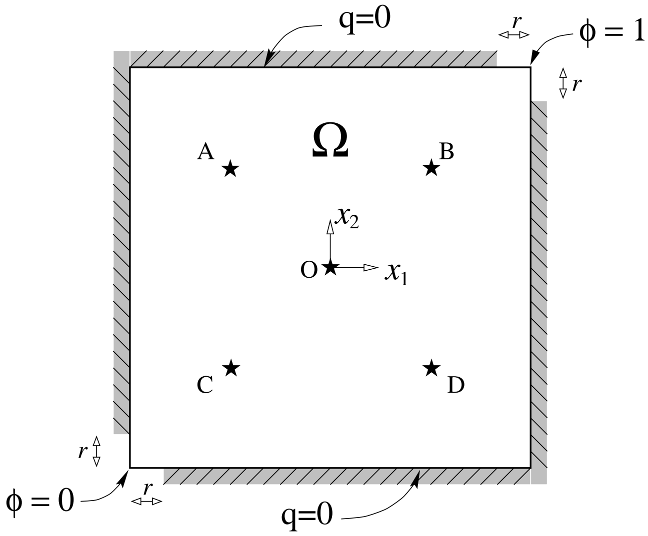

Figure 13

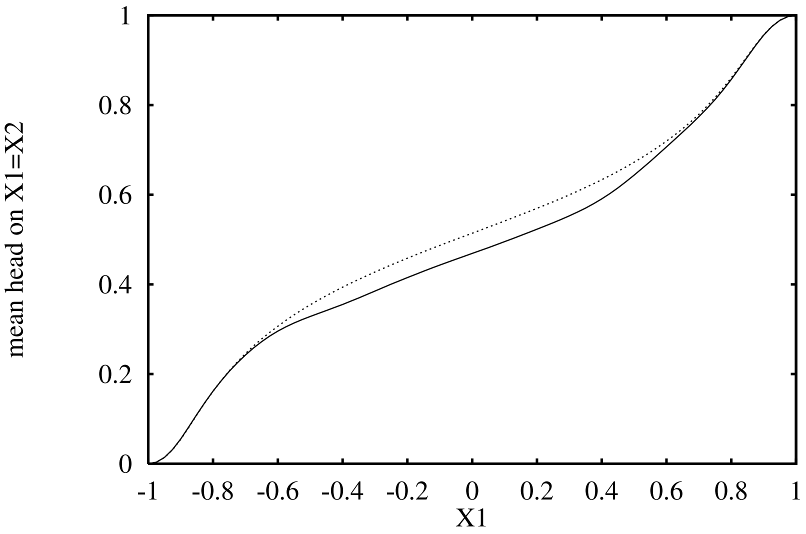

Figure 14

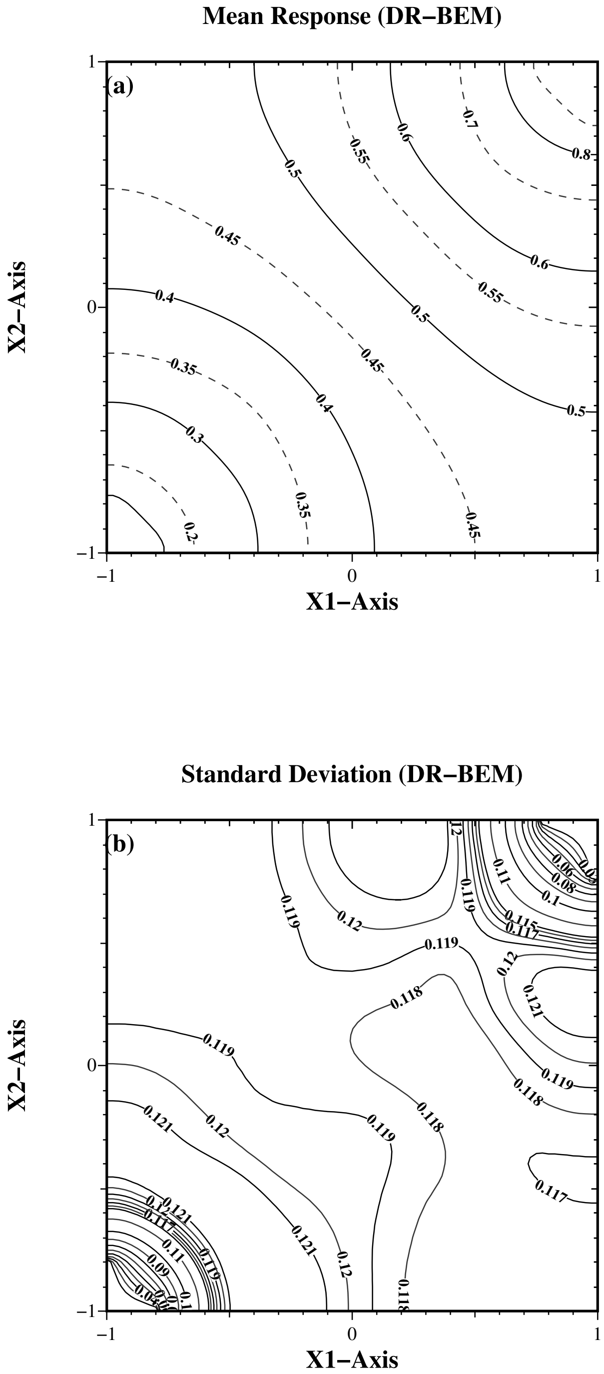
Mean Response (DR−BEM)
(a)
X2−Axis
X1−Axis
0.2
0.3
0.35
0.4
0.45
0.5
0.55
0.6
0.7
0.8
Standard Deviation (DR−BEM)
(b)
X2−Axis
X1−Axis
0.117
0.118
0.119
0.12
0.121

Figure 15

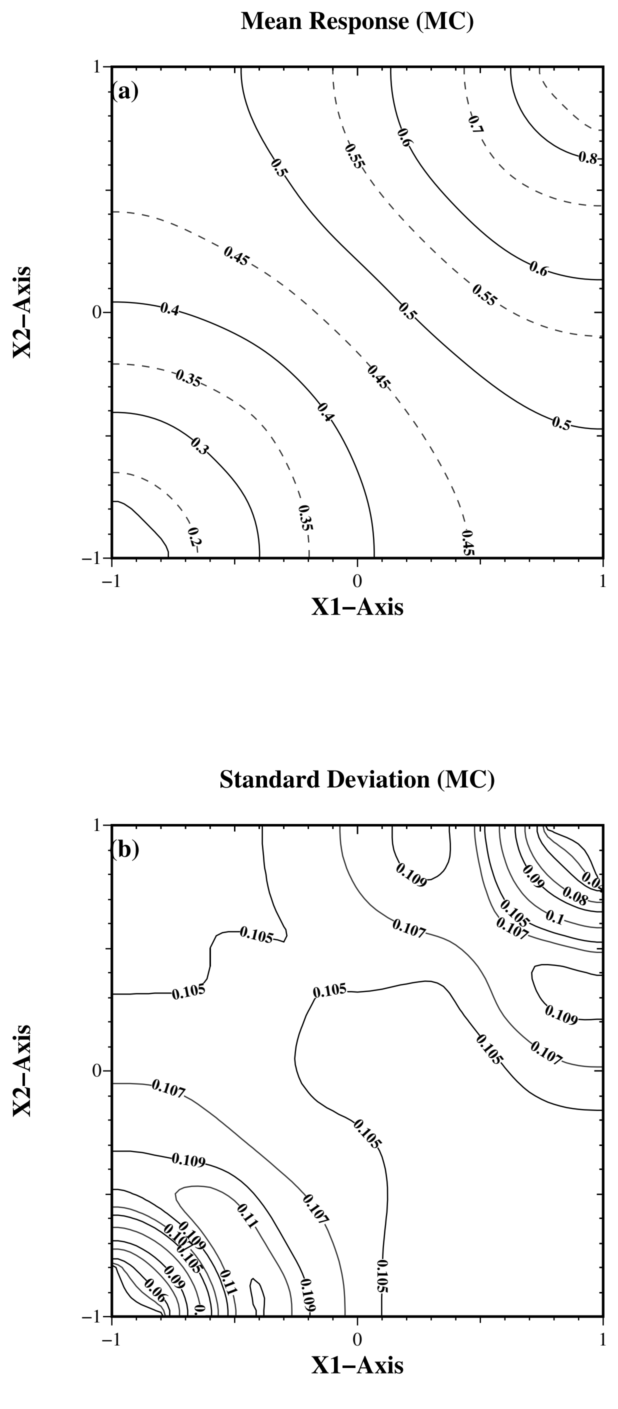
Mean Response (MC)
(a)
0.2
0.3
0.35
0.4
0.45
0.5
0.55
0.6
0.7
0.8
X1−Axis
X2−Axis
−1
0
1
Standard Deviation (MC)
(b)
0.06
0.08
0.09
0.1
0.105
0.107
0.109
0.11
X1−Axis
X2−Axis
−1
0
1

Figure 16